

Review

Carbon Nanotube Fiber-Based Wearable Supercapacitors—A Review on Recent Advances

Kavitha Mulackampilly Joseph ¹, Hunter J. Kasparian ² and Vesselin Shanov ^{1,2,*} ¹ Department of Mechanical and Materials Engineering, University of Cincinnati, Cincinnati, OH 45221, USA² Department of Chemical and Environmental Engineering, University of Cincinnati, Cincinnati, OH 45221, USA

* Correspondence: shanovvn@ucmail.uc.edu

Abstract: As wearable electronic devices are becoming an integral part of modern life, there is a vast demand for safe and efficient energy storage devices to power them. While the research and development of microbatteries and supercapacitors (SCs) have significantly progressed, the latter has attracted much attention due to their excellent power density, longevity, and safety. Furthermore, SCs with a 1D fiber shape are preferred because of their ease of integration into today's smart garments and other wearable devices. Fiber supercapacitors based on carbon nanotubes (CNT) are promising candidates with a unique 1D structure, high electrical and thermal conductivity, outstanding flexibility, excellent mechanical strength, and low gravimetric density. This review aims to serve as a comprehensive publication presenting the fundamentals and recent developments on CNT-fiber-based SCs. The first section gives a general overview of the supercapacitor types based on the charge storage mechanisms and electrode configuration, followed by the various fiber fabrication methods. The next section explores the different strategies used to enhance the electrochemical performance of these SCs, followed by a broad study on their stretchability and multifunctionality. Finally, the review presents the current performance and scalability challenges affecting the CNT-based SCs, highlighting their prospects.

Keywords: carbon nanotube fiber; energy storage; wearable technologies; supercapacitor; fiber spinning



Citation: Joseph, K.M.; Kasparian, H.J.; Shanov, V. Carbon Nanotube Fiber-Based Wearable Supercapacitors—A Review on Recent Advances. *Energies* **2022**, *15*, 6506. <https://doi.org/10.3390/en15186506>

Academic Editors: Huang Zhang and Yuan Ma

Received: 1 August 2022

Accepted: 1 September 2022

Published: 6 September 2022

Publisher's Note: MDPI stays neutral with regard to jurisdictional claims in published maps and institutional affiliations.



Copyright: © 2022 by the authors. Licensee MDPI, Basel, Switzerland. This article is an open access article distributed under the terms and conditions of the Creative Commons Attribution (CC BY) license (<https://creativecommons.org/licenses/by/4.0/>).

1. Introduction

Wearable electronics have become indispensable in modern life, with rapid advances in the devices and their applications, such as in displays, fitness trackers, body-mounted sensors, artificial intelligence (AI) hearing aids, virtual reality (VR) headsets, and smart textiles. These devices require equally flexible, wearable, and high-performance energy storage devices to maintain their performance and safety. Unfortunately, most conventional 3D energy storage devices are stiff, rigid, heavy, and bulky. Therefore, recently a rapid shift has been seen from 3D to 2D planar-type energy storage devices in the form of metal-coated plastics, cloths or fabrics coated with conductive carbon, and conductive papers, which are flexible, portable, and lightweight. However, they were proven to be uncomfortable as wearable devices as they lacked the flexibility to conform to various body types and could not comply with the breathability requirements (to allow circulation of air passage between the body and the garment) [1–5]. Therefore, fiber-based 1D energy storage devices with desirable flexibility, lighter weights, smaller volumes, and conformability are the most promising solution for mitigating the abovementioned issues [6,7].

Supercapacitors (SCs) are superior to conventional SCs in energy density and are superior to batteries in terms of power delivery. One of the most appropriate chemical elements suitable for electrochemical capacitor applications is carbon, due to its high electrical conductivity, mechanical strength, wide natural presence, low density, and controllable structure and properties. Being placed in the middle of the eight-element period in the periodic table, it exhibits moderate electronegativity, with an electronic structure ($1S^2, 2S^2, 2P^2$)

and four valence electrons. Various forms of carbon, such as carbon black, natural or artificial graphite, carbon nanotubes (CNTs), graphene, and activated carbon, are substantially used in commercial SCs as conductive additives or active materials. However, most of them are applied as conductive coatings and films on metallic supports consolidated with binders, thereby making the SCs often bulkier, heavier, and non-flexible.

On the other hand, CNT-fiber-shaped SCs are long in size, mechanically robust, and have a tunable structure. They are macroassemblages of CNTs in the 1D fiber form. They can integrate all of the desirable features of fiber-based SC, such as extraordinary electrical conductivity, mechanical strength, flexibility, tunable porosity and surface area, and excellent stability. These unique energy storage devices are also self-standing, binder-free, and can be easily integrated into textiles and wearable devices [5,7–9].

Wearable supercapacitors represent a hot research topic, and recently there have been excellent reviews regarding supercapacitors [2,10–12], microsupercapacitors [13], flexible supercapacitors [14,15], carbon-based supercapacitors [16–18], and fiber-based supercapacitors [1,4,7,9,19,20]. However, the reviews on carbon nanotube fiber-based SCs are scarce [5,21,22]. These publications present significant studies on fiber spinning, energy conversion, novel fiber fabrication methods, and smart applications of CNT yarn. However, a comprehensive review discussing the fundamental aspects and the recent advances of CNT-based SCs is still in demand. The initial sections of the current review focus on the SCs' fundamentals, including the types of SCs based on the charge storage, configuration, and fabrication method. The next section explores strategies that can be adopted for the greater performance of CNT electrodes and CNT fiber SCs as a whole, followed by a study on 'stretchable' and 'multifunctional' CNT-based SCs. Finally, the review analyzes the challenges of CNT-based SCs, followed by exploring the prospects of these energy storage devices.

2. Background and Fundamentals of Supercapacitors

Historically, the idea of storing electrical energy became a reality with the invention of the Leyden jar in 1746. However, the concept of using stored energy for practical purposes arose only in 1954 when Becker was granted a patent for storing electrical energy in a battery or cell. The patent claims the electrical energy storage at the interface of a porous carbon electrode and aqueous electrolyte in the form of a double layer [6].

Supercapacitors are devices that can store and release electrical energy by quickly transferring the charge in the form of electrons and ions during the charge and discharge process. The conventional form of a supercapacitor consists of two parallel plates, one positive and the other negative, with a thin insulating membrane between them called the dielectric (Figure 1a). The charge stored is in the form of potential energy between the plates. The electrolytic capacitor is the next-generation capacitor, where the thin insulator is replaced by an ionic conductive medium called an electrolyte, in which the ions are free to move. The free movement of ions in the bulk of the electrolyte provides a higher charge density. The capacitance obtained from an electrolytic capacitor is much greater (mF range) compared to a conventional dielectric capacitor (μF range). Supercapacitors (SCs) or ultracapacitors, also known as electrochemical capacitors, consist of two electrodes connected ionically through an electrolyte and separated by an ion-permeable membrane called a separator made of polymer, paper, fiber, glass, ceramic, or cardboard (Figure 1b). High specific capacitance rates (tens of farads instead of mfarads) are possible with these devices obtained from a minimal volume of 1 cm^3 . Because of this quality, they are also called ultracapacitors. The key reasons for the high capacitance achieved are due to the two different charge storage mechanisms involved: (a) an electric double-layer capacitor (EDLC), utilizing a large surface area in porous carbon materials; and (b) a mechanism utilizing reversible redox reactions, as in the case of pseudocapacitive materials [3,6,23,24].

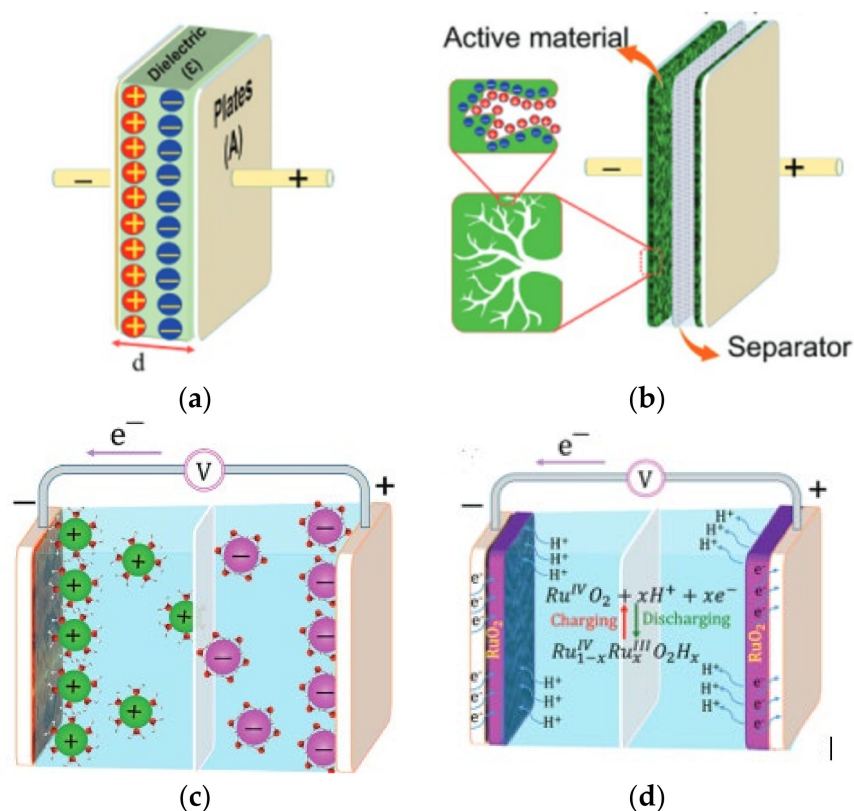


Figure 1. Schematics of (a) conventional capacitor, (b) supercapacitor, (c) electric double layer capacitor (EDLC), and (d) pseudocapacitor. Reproduced with permission from [24].

2.1. Type of SCs Based on Charge Storage

EDLCs are electrochemical double-layer capacitors (Figure 1c) that store the charge on the surface through double-layer charging. The double layer is formed by the quick adsorption–desorption of ions on the active electrode surface during charge–discharge. When power is applied to the system, a double-layer charge is formed at each electrode–electrolyte interface without any charge transfer. The process is non-Faradaic because there is no change in chemical composition or phase, and it is reversible, which renders the capacitors with high cycling stability [17].

For such capacitors, the capacitance at each electrode is given by:

$$C_e = \frac{\epsilon S}{d} \quad (1)$$

where ϵ is the permittivity of the dielectric constant, S is the surface area of the electrode–electrolyte interface, and d is the EDL thickness.

As d is usually in the nanometer range and the surface area is directly proportional to the specific capacitance, the ideal candidates for supercapacitors are nanoporous carbons with the advantage of a very large specific surface area (SSA) in the range of $1000\text{--}2500 \text{ m}^2\cdot\text{g}^{-1}$ high electrical conductivity, and low cost. Activated carbon (AC), nanocarbons (CNTs, graphene), and nanoporous metals can provide superior capacitance via double-layer charging due to having a larger surface area [6].

In pseudocapacitors (Figure 1d), the charge storage is achieved via redox or Faradaic reactions occurring at the surface of the electrode without ion diffusion. As a result, pseudocapacitors give a higher capacitance and energy density than carbon-based EDLCs. The cause of the pseudocapacitance can be due to various mechanisms such as redox reactions, intercalation, doping, and underpotential deposition, as illustrated in Figure 2.

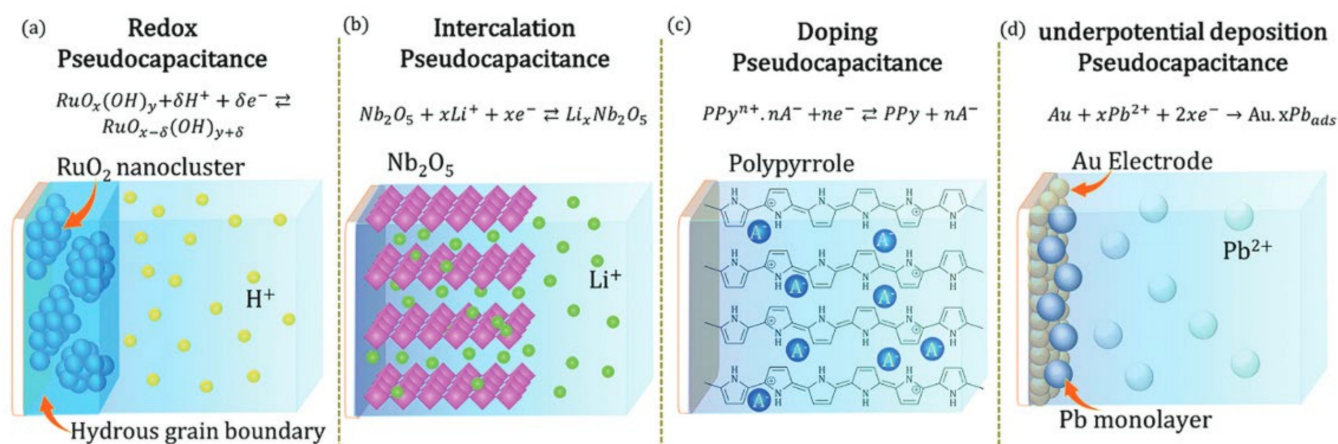


Figure 2. Scheme of different types of redox reactions giving rise to pseudocapacitance. Reproduced with permission from [24].

Metal oxides, nitrides, hydroxides, and sulfides and conducting polymers such as polyaniline, polypyrrole, and polythiophene are pseudocapacitive materials. These materials are mostly hybridized with carbon materials to improve the available capacitance and cyclic stability, because carbon-based materials can enhance the conductivity and stability [4,7,12]. Table 1 compares the different pseudocapacitor material types, showing their advantages and drawbacks.

Table 1. Comparison of different pseudocapacitor material types.

Pseudocapacitor Type	Advantages	Drawbacks
Transition metal oxides		
RuO ₂	<ul style="list-style-type: none"> • High specific capacitance • High-rate capability • High proton conductivity • Wide potential window • Long cycle life 	<ul style="list-style-type: none"> • High cost • Environmental hazard
MnO ₂	<ul style="list-style-type: none"> • Outstanding theoretical specific capacitance (1370 F·g⁻¹) • High oxygen evolution potential • Low cost • Abundance in nature • Environmentally friendly • Easy synthesis • Good electrochemical performance (especially in aqueous and neutral electrolytes) 	<ul style="list-style-type: none"> • Low conductivity • Low-rate capability • Insufficient cyclic stability owing to MnO₂ dissolution • Broad band gaps • Low ionic diffusion coefficient
V ₂ O ₅	<ul style="list-style-type: none"> • Can be used as a pseudocapacitive electrode in neutral and aqueous electrolytes • Easy preparation. It can be prepared via electrodeposition, sol-gel, hydrothermal, and quenching methods. 	<ul style="list-style-type: none"> • Low specific surface area • Low solubility (limits the specific capacitance improvement)

Table 1. Cont.

Pseudocapacitor Type	Advantages	Drawbacks
Iron-based materials (Fe ₂ O ₃ , Fe ₃ O ₄) & (FeC ₂ O ₄), FeOOH	<ul style="list-style-type: none"> Natural abundance Low cost Environmental friendliness High theoretical capacitance 	<ul style="list-style-type: none"> Difficult to transfer theoretical values into practical applications due to Relatively small surface area Low electrical conductivity Poor rate performance Limited cyclic stability
Oxides/hydroxides of Ni/Co	<ul style="list-style-type: none"> Simple preparation High theoretical specific capacitance in basic electrolytes 	<ul style="list-style-type: none"> The strong alkaline nature probably hinders practical applications in future wearable electronics
Other oxides (InO ₂ , WO ₃ , MoO ₃ , SnO ₂)	<ul style="list-style-type: none"> Good electrochemical performance 	<ul style="list-style-type: none"> Poor conductivity/Slow kinetics/difficult to synthesis/Unstable
Transition metal sulfides		
(MoS ₂ , FeS/Cos/CuS, NiS)	<ul style="list-style-type: none"> High electrical conductivity High specific capacitance High mechanical and thermal stability 	
Transition metal nitrides		
	<ul style="list-style-type: none"> High electrical conductivity (4000–5500 S·cm⁻¹) Better sustainability than metal oxides 	<ul style="list-style-type: none"> Synthesis demands strict operating conditions that are incompatible with wearable electronic components
Vanadium Nitride (VN)	<ul style="list-style-type: none"> High theoretical specific capacitance (1340 F·g⁻¹) Remarkable electrical conductivity (1.67 × 10⁶ Ohm·m) unlike other anodes such as carbon-based materials, MoS₂, and Fe₂N Large potential window Fast reversible redox reaction 	<ul style="list-style-type: none"> Mismatch between theoretical and experimental values of capacitance

Conductive polymers (CP) are potential candidates for future wearable electronics energy storage devices due to their inherent polymeric elastic nature, good electrical conductivity, and capability to undergo fast and reversible redox reactions. CPs become good conductors after doping and have a low equivalent series resistance. As a result, they experience quick redox reactions yielding good capacitance. They also have a wide voltage window leading to high energy density. CPs also enable the storage of charges without structural and phase changes. This allows for greater capacitance due to a larger surface area and a greater charge storage capacity.

CPs undergo redox reactions due to the presence of conjugated pi electrons. The ions travel to the backbone of the polymer during doping or oxidation and move back to the electrolyte during de-doping or reduction. Table 2 discusses the advantages and drawbacks of popular CPs used for energy storage devices [4,7,12].

Table 2. Comparison of different conductive polymers.

Type of Conducting Polymer	Advantages	Drawbacks
PANI	<ul style="list-style-type: none"> • High electronic conductivity • Redox and ion-exchange properties resulting in high capacitance • Ease of preparation • Excellent environmental stability • Lightweight • Low cost • High flexibility • Environmental friendliness 	<ul style="list-style-type: none"> • Mechanical stress during charge–discharge leads to poor cycle life
PEDOT-PSS	<ul style="list-style-type: none"> • High conductivity • High redox active • Good chemical and electrochemical stability • Ease of preparation 	<ul style="list-style-type: none"> • Low specific capacitance due to high molecular weight and low doping level.
Polypyrrole (PPY)	<ul style="list-style-type: none"> • Conductivity in the range of 10–500 S·cm^{−1} • Better rate capability • More flexible and denser than other CPs. 	<ul style="list-style-type: none"> • Unable to be doped with n-doped materials, hence its application is limited to cathode of SCs

2.2. Supercapacitor Designs

A supercapacitor can have different designs based on the types of electrodes. A symmetric supercapacitor consists of an anode and cathode made of the same material, and carbon materials are commonly used. In contrast, an asymmetric supercapacitor can have various combinations of electrode materials, as shown in Figure 3 [24].

A hybrid capacitor is a combination of two electrode types—one a capacitive type and the second a capacitive Faradaic (pseudocapacitive) or non-capacitive Faradaic type (battery type). Combining both capacitive and Faradaic kinds of electrodes helps to achieve higher energy and power densities greater than EDLC devices, while also providing better cyclic stability and affordability, the absence of which has hindered the wide usage of pseudocapacitors in the past.

2.3. Performance Metrics of Supercapacitors

The capacitance of a supercapacitor system (C) is given by:

$$\frac{1}{C} = \frac{1}{C_1} + \frac{1}{C_2} \quad (2)$$

In the charged state, the two electrodes with capacitance C_1 and C_2 act like two capacitors in series. The electrode with the lower capacitance determines the capacitance of the system.

A supercapacitor's energy density or specific energy (E) is the amount of energy stored per unit mass, volume, or area of the active electrode materials or the whole device.

$$E = \frac{1}{2}CU^2 \quad (3)$$

where U is the operating voltage.

The specific power or power density (P) is the amount of power a supercapacitor can deliver per unit mass, volume, or area of the electrode's active materials or the whole device [17].

$$P = \frac{U^2}{4R_S} \quad (4)$$

where R_S is the equivalent series resistance of the supercapacitor. The performance of an energy storage device is determined by the Ragone plot, which expresses the relation between the specific energy and specific power (Figure 4).

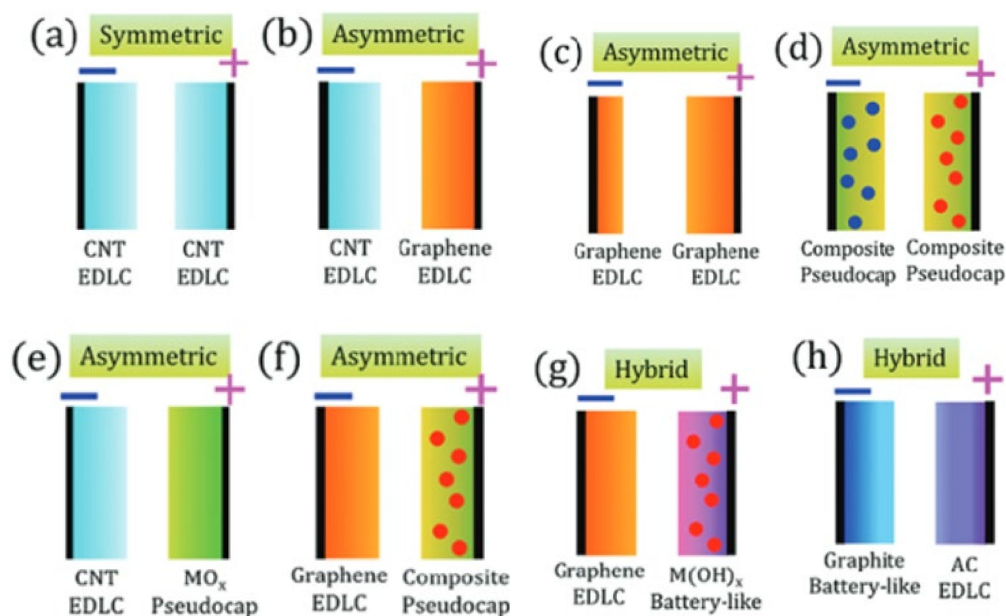


Figure 3. Schematic representation of the symmetric, asymmetric, and hybrid configurations. (a) Symmetric supercapacitor. As shown in the figure, asymmetric supercapacitors cover a wide range of electrode combinations, including (b) two different EDLC electrodes (c) with the same material at both electrodes but different mass loadings, (d) two pseudocapacitive electrodes with different compositions, (e) one EDLC electrode with a pseudocapacitive electrode (e.g., an activated carbon/MnO₂ aqueous supercapacitor), (f) one EDLC electrode with a composite electrode (that can be a composite of carbon-based materials with a metal-based species), (g) a hybrid configuration that is fabricated using a capacitor-type negative electrode and a battery-like positive electrode, and (h) a hybrid architecture (typical of a Li-ion capacitor) that is fabricated using a battery-type negative electrode and an EDLC positive electrode. Reproduced with permission from [24].

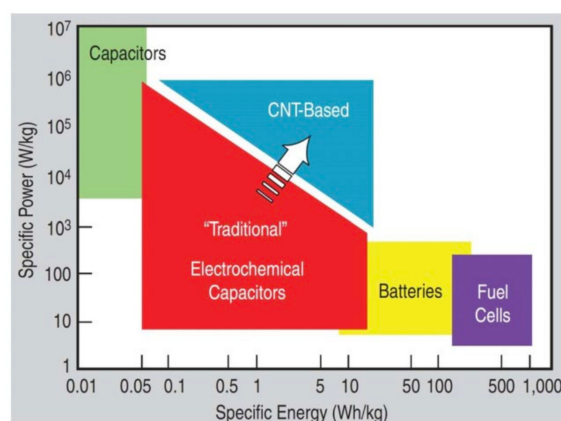


Figure 4. Ragone plot for the current generation of capacitors, supercapacitors, batteries, and fuel cells. Reprinted with permission from [25].

From the Ragone plot, it can be observed that the electrochemical capacitors have higher specific power levels than batteries and fuel cells but lower energy densities than them. Therefore, the current research is focused on designing supercapacitors with higher energy density without compromising on their excellent power density. Additionally, it can be noted from Figure 4 that carbon-nanotube-based electrochemical capacitors have superior power and energy properties over other electrochemical capacitors.

3. CNT Fiber for SCs

Carbon nanotubes (CNTs) are apt candidates with an SP^2 hybridized carbon, possessing all of the desired properties for a wearable SC. Due to the 1D nanostructure, they can be easily assembled into a 1D fiber. Furthermore, the CNTs retain high mechanical strength and flexibility and an exceptional specific surface area when assembled from the nanoscale to macroscopic scale in the fiber form. With all of these attributes, CNT assemblages in the fiber form can simultaneously be used as fiber scaffolds, current collectors, and active material electrodes for wearable SCs [5,7,8].

3.1. Fabrication of CNT Fibers

The macroscopic assemblage of CNT fibers from nanoscale carbon can be accomplished without complex treatments such as carbonization, which is an added advantage of the CNT fiber fabrication. The fabrication can be accomplished via (1) wet spinning from CNT dispersions, (2) dry spinning from CNT aerosols, (3) dry spinning from CNT arrays or forests, and (4) the twisting of CNT thin films. The CNT fiber's electrical, mechanical, and electrochemical properties depend on the fiber morphology (the structural alignment and pore structure). The fiber morphology, in turn, is determined by the assembly methods and related process parameters.

3.1.1. Wet Spinning from Dispersions

The wet spinning of CNT fibers from dispersions is a scalable process that has been practiced since 2000 [26]. It is usually accomplished by preparing a homogenous dispersion of CNTs with a surfactant or polymer and extruding it into a coagulation bath. The extruded flow becomes a solidified fiber enabled by the nanomaterials' agglomeration during the fiber's wet drawing. The latter is accomplished using a rotating spool, a rotating coagulation bath, or fiber gravity. The obtained fiber is mechanically strong but exhibits poor electrical and thermal properties due to the presence of the polymer. Polymer-free dispersion and spinning processes have also been succeeded tested, as reported by Behatbu in 2013 and Bucossi in 2015 [27,28]. The fiber morphology and fiber properties can be fine-tuned via the optimization of the wet spinning parameters, which include the following:

- The extrusion speed;
- The needle or spinneret diameter and shape;
- The quality and concentration of spinning dispersion;
- The rotation speed in the rotated spinning method;
- The nature of the coagulation bath (fast coagulation results in a non-homogenous structure, while slow coagulation imparts a homogenous structure);
- The drawing speed and ratio (a higher ratio improves the alignment, strength, and fiber conductivity);
- The post-treatment, if any (such as annealing, which is used to remove the oxides to make the fibers more conductive).

Kou et al. demonstrated a coaxial wet spinning process [29] to achieve a higher capacitance and rate capability using CNTs and reduced graphene oxide (RGO) as the spinning dope. In the coaxial spinning process, the spinneret consists of two inlets, one for the core and the other for the sheath, as shown in Figure 5a.

The core combines CNTs and RGO; the sheath is made of sodium carboxy methyl cellulose (CMC). The polyelectrolyte (CMC) acts as an ion-permeable membrane but is insulative to the electron flow. An electrode RGO+CNT@CMC is spun with a GO and CNT

mixture (w/w , 1/1) of 20 mgml⁻¹ and CMC 8 mgml⁻¹. SEM images of the coaxial fiber can be seen in Figure 5b–d. Two coaxial fiber electrodes (CNT + RGO @ CMC) are intertwined to form a two-ply yarn SC with a layer of PVA-H₃PO₄ gel electrolytes (Figure 5e–g). The CMC sheath layer protects the SC from short circuits. The SC yarn with a mixture of RGO + CNT outperformed the other SC with only RGO @ CMC and CNT @ CMC. The aerial capacitance C_A of CNT + RGO @ CMC exhibited superior capacitance of 177 mFcm⁻² (158 F/cm³) at a current density of 0.1 mA/cm², whereas the C_A values for RGO@ CMC and CNT@CMC were 39 mF/cm² and 127 mF/cm², respectively. The higher capacitance could be attributed to the higher surface area formed by the synergistic combination of CNT and RGO. Additionally, the superior electrochemical performance could be due to the lower internal resistance, as confirmed via electrochemical impedance spectroscopy (EIS) and shown in Figure 5i.

To assess the advantage of the coaxial spinning process, the authors fabricated a control yarn SC via the conventional wet spinning of CNT + RGO dispersions and further coated it with CMC. They also reported that the coaxial-spun SC exhibited a capacitance of 103 mF/cm². In contrast, the conventionally spun and post-coated SC yarn gave a much lower capacitance rate of 39 mF/cm² at a current density of 0.1 mA/cm². The main reason is that the coagulation and drying of the outer CMC layer during the spinning process are faster than for the core, which leads the sheath to tightly wrap around the core, resulting in better ion transport between the electrolyte and electrode. Additionally, the pore formation in the CNT and GO inner core during the spinning process is complicated due to the uniform shrinkage of the CMC layer. A thicker layer increases the shrinkage force, which affects the pore structure. Therefore, a thicker CMC provides higher capacitance to the SC. Finally, it can be noted that the CMC has no pseudocapacitive effect in the process, and the improved performance can be attributed to the coaxial spinning process.

Wet Spinning and Incorporation of Pseudocapacitive Materials

SCs based on nanocarbon usually exhibit limited capacitance because double-layer electrochemical charging is the only charge storage mechanism. Therefore, combining pseudocapacitive materials such as metal oxides and conducting polymers with carbon is standard practice. Furthermore, wet spinning methods are advantageous because they allow the easy incorporation of such active materials in the spinning dispersions, providing composite CNT electrodes with the required electrochemical performance and other functionalities.

I. Metal oxides

Lu et al. [30] synthesized SCs with high mechanical strength and superior electrochemical performance in the wet spinning of a liquid crystal dispersion containing single-walled CNTs and by further electrodepositing MnO₂. The “as-spun” single-wall carbon nanotubes (SWCNTs) had a tensile strength and conductivity of 225 MPa and 450 ± 15 S·cm⁻¹, respectively. These values were 246% and 50% higher than the previously reported fibers. The reason could have been the highly aligned SWCNTs and the low contact resistivity between the CNT bundles. Further, MnO₂, which has high theoretical capacitance, was electrodeposited on SWCNT fibers to form a MnO₂/SWCNT hybrid electrode. Two electrodes contained PVA/LiCl as the electrolyte to form a parallel symmetric SC. As reported by the authors, the SC exhibited an energy density of 14.1 Wh·kg⁻¹ and a power density of 202 W·kg⁻¹, and showed an increased capacitance of 16% after 10,000 cycles. The impressive electrochemical performance was attributed to the fast ion transport made possible by the uniformly deposited mesoporous MnO₂ nanoflakes on the well-aligned, highly conductive CNT fiber.

The method of active material loading via post-deposition on CNT fibers has limitations for high loading rates. In contrast, the pre-deposition of the active material on a vertically aligned carbon nanotube (VACNT) array, which is then twisted into a fiber, is complicated and time-consuming. Therefore, Li et al. [31] tried using a conventional wet spinning process to fabricate a hybrid SWCNT/MnO₂ fiber, in which the aqueous

dispersions of SWCNTs and MnO_2 were mixed with the help of the surfactant sodium chloride, and were then spun, washed, and dried. The SWCNT/ MnO_2 hybrid fiber had a 75% mass loading rate, conductivity of $761 \text{ S}\cdot\text{cm}^{-1}$, and volumetric capacitance of $74.8 \text{ F}/\text{cm}^3$. Furthermore, an SC fabricated in a parallel symmetric configuration using the hybrid fiber gave an energy density of $10.4 \text{ mWh}\cdot\text{cm}^{-3}$ at a power density of $0.05 \text{ W}\cdot\text{cm}^{-3}$ and exhibited good cyclic stability (94% capacitance retention in 5000 cycles). According to the authors, the superior performance was due to the highly loaded conductive hybrid fiber facilitating quick electrical pathways thanks to the close contact between the SWCNT and MnO_2 nanosheets and the hierarchical pore structure helping the faster ion transport.

Since the conductivity of the MnO_2 used as pseudocapacitive material is low, Kim et al. [32] identified a solution incorporating platinum nanoparticles (PtNP) with MnO_2 through a one-step scalable wet spinning process to produce CNT/ MnO_2 /PtNP composite electrodes. CNT powder, MnO_2 powder, Pt nanoparticles, and water are mixed together and injected into a coagulation bath of PVA/water. The process is scalable; however, greater the length, the greater the resistance. The added Pt nanoparticles increased the conductivity, the PVA enhanced the mechanical strength, the CNT acted as a mechanically stable conductive core, and the MnO_2 provided the necessary pseudocapacitance. Two parallel electrodes coated with PVA-LiCl fabricated as an SC exhibited a capacitance of $53.1 \text{ mF}\cdot\text{cm}^{-2}$ at $10 \text{ mV}/\text{s}$, an energy density of $1.84 \text{ }\mu\text{Wh}\cdot\text{cm}^{-2}$, and a power density of $13.3 \text{ }\mu\text{W}\cdot\text{cm}^{-2}$. The capacitance was 49 times higher than for CNTs in a bare SC due to the presence of conductive Pt nanoparticles, which also reduced the resistance. The rate capability was retained at 60% when the scan rate varied from 10 to 100 mV/s.

II. Conducting polymers

Meng et al. [33] demonstrated the wet spinning of stable dispersions of SWCNTs and polyaniline nanowires (PANI NWs) with an outer PVA sheath. These flexible and highly conductive electrodes were combined with a PVA- H_3PO_4 electrolyte to make twisted yarn SCs. The yarn SCs with the composite SWCNT/PANI NWs exhibited 18-fold more capacitance than the SCs based on bare SWCNTs.

Zheng et al. [34] fabricated a core–sheath SC electrode with the core being hyaluronic acid (HA) and with CNTs and electrodeposited PANI as the sheath. While HA acts as a biocompatible surfactant to improve the dispersion of CNT during wet spinning, it also serves as an ion-conducting binder. PANI is deposited on the fiber via electrochemical polymerization. The authors presented data showing that the HA/CNT/PANI electrode revealed a 6-fold greater specific capacitance than the HA/CNT core. In contrast, the HA/CNT core provided high levels of electrical conductivity, mechanical robustness, and stiffness. The authors claimed the electrode's superior mechanical, electrical, and electrochemical performances were due to the in situ polymerization of PANI, which facilitates hydrogen bonding between the carboxyl groups of HA and amine groups of PANI. They also reported it as having high cyclic stability (90% capacitance retention after 3000 cycles at $100 \text{ mV}/\text{s}$). The high-performing, low-cost electrode was possible not only due to the synergistic interaction between the HA/CNT core and PANI sheath but also thanks to the interaction and alignments of the HA/CNT core–sheath, including the favorable pore structure and high specific surface area of the PANI.

III. Metal oxides and conducting polymers

Torres et al. studied [35] a mixture of carbon black (CB), CNT, and chitosan dispersions which were wet-spun to form a carbon skeleton, after which the MnO_2 (of two different crystalline structures, ϵMnO_2 and γMnO_2) was electrodeposited, followed by dip coating to form a layer of poly(3,4-ethylene dioxythiophene) (PEDOT) conducting polymer or polypyrrole. Finally, symmetric SCs were fabricated from various combinations of the above electrodes shown in Table 3, resulting in high capacitance and cyclic stability rates.

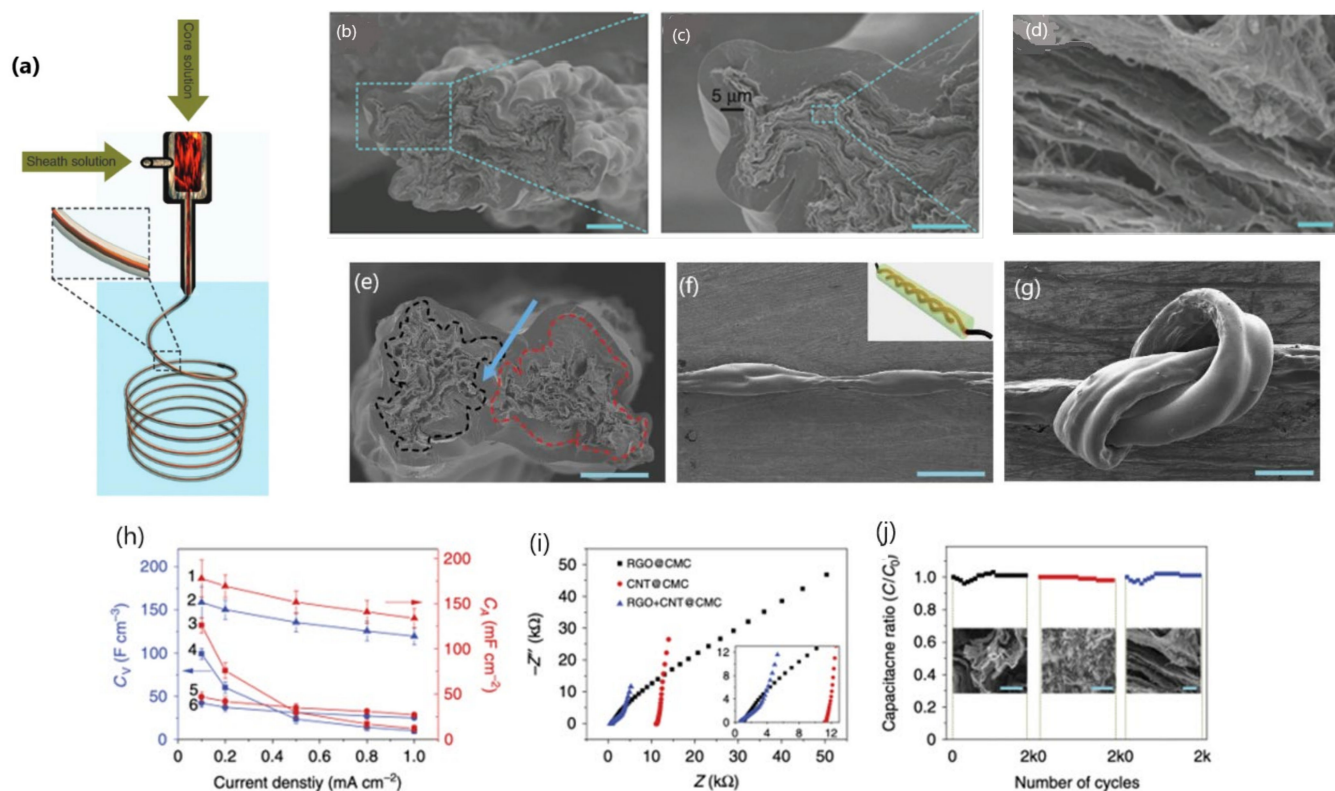


Figure 5. The coaxial wet spinning assembly process, showing fabricated yarn SCs (YSCs), their morphology, and their electrochemical performance. (a) Schematic of coaxial spinning. (b–d) SEM images of RGO + CNT@CMC. (e–g) SEM images of two-ply SCs in (e) cross-sectional view and (f) side view. The arrow in (e) is a PVA/H₃PO₄ electrolyte, and the inset of (f) shows the schematic illustration of the yarn SCs. (g) SEM image of a two-ply yarn SC knot. (h–j) Electrochemical performances of yarn SCs, (h) with the dependence of CA and CV on the charge–discharge current density for RGO@CMC (3, 4), CNT@CMC (5, 6), and RGO + CNT@CMC (1, 2) YSCs. (i) Nyquist plots, (j) showing the normalized capacitance (C/C_0 , where C_0 is the initial capacitance) versus cycle number for RGO@CMC (left), CNT@CMC (middle), and RGO + CNT@CMC (right) YSCs. Scale bars: 20 μm for (b), 10 μm for (c), 0.2 μm for (d), 50 μm for (e), 500 μm for (f), 200 μm for (g), 3 mm for left, and 0.3 mm for middle and right (j). Reproduced with permission from [29].

Table 3. Fabrication steps to make symmetric supercapacitors. Reproduced with permission from [35].

1st Step: Wet Spinning	2nd Step: MnO ₂ Electrodeposition	3rd Step: Coating of Conducting Polymer	Electrodes
CB-CNT fibers	Mn(CH ₃ COO) ₂	PEDOT	MnAc ₂ -PEDOT
	Mn(CH ₃ COO) ₂	PPY	MnAc ₂ -PPY
	Mn(NO ₃) ₂	PEDOT	Mn(NO ₃) ₂ -PEDOT
	Mn(NO ₃) ₂	PPY	Mn(NO ₃) ₂ -PPY

The SC with PEDOT gave a high capacitance fiber, while the one with polypyrrole revealed higher cyclic stability. Therefore, to obtain both in a single SC, the Mn(CH₃COO)₂/PEDOT fiber was coated with polypyrrole (PPY). As a result, the cyclic stability improved from 79% to 89%, and the capacitance obtained was maintained at 549 F/g. Thus, this study proves the opportunity for tuning the SC components from the different layers available (MnO₂, PEDOT/polystyrene sulfonate/PSS, PPY).

3.1.2. Dry Spinning from CNT Aerosols

In this process, the precursor carbon source (organic vapor or solid carbon) decomposes at a very high temperature to produce carbon atoms. These grow into CNTs with the help of catalyst nanoparticles formed in situ and floating in the vapor. With the help of van der Waals forces or pi-pi interactions, the formed CNTs self-assemble into an aerogel or network of nanobundles. These can be collected as long fibers on a spindle or as a ribbon, or on a rotating drum [36]. The number of walls, diameter, and length of the CNTs can be controlled by fine-tuning the following process parameters:

- The carbon precursor;
- The catalyst concentration;
- The rate of hydrogen gas flow;
- The temperature of the pyrolysis.

The fiber morphology and mechanical and electrical properties can be optimized by controlling the following aspects:

- The CNT alignment, length, and structure;
- The post-treatment;
- The rate of the gas flow;
- The speed of the winding;
- The presence of particulate impurities and defects.

Li et al. [37] grew ultra-long and well-aligned CNT fibers by winding the CNT aerogel continuously, which was produced using the floating CVD process. A schematic of the CNT floating catalyst CVD process is shown in Figure 6.

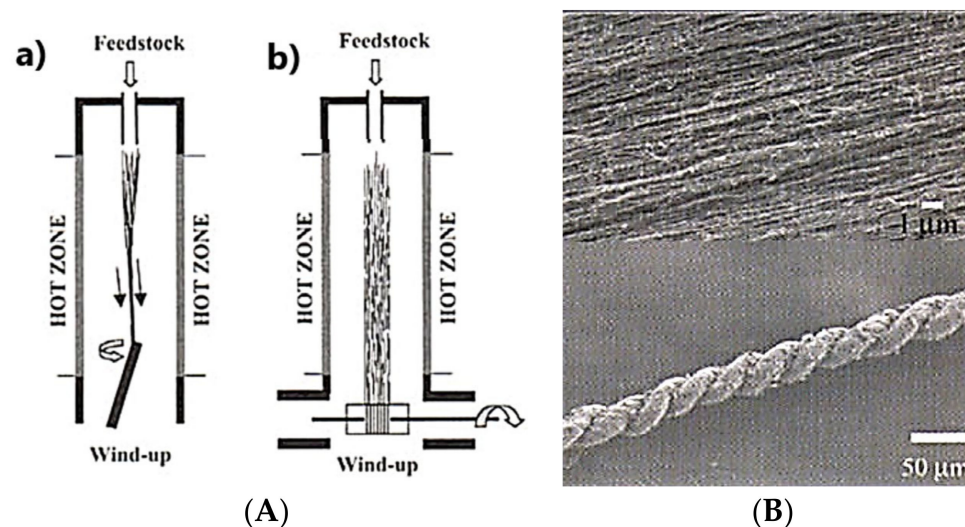


Figure 6. (A) (a) Schematic of the direct spinning process, called the floating catalyst CVD process. Liquid feedstocks such as ferrocene and thiophene are dissolved in ethanol, mixed with H_2 , and then injected into a hot zone where the CNT aerogel is formed. This aerogel is captured and wound out of the hot zone by an offset rotating spindle. (b) Schematic of the wind-up assembly operating at a lower temperature, outside the furnace hot zone. (B) SEM images of well-aligned multiwall carbon nanotubes (MWCNTs) along with a twisted fiber collected from the furnace. Reprinted with permission from [37].

3.1.3. Dry Spinning from CNT Arrays

In this method, the CNT fiber is drawn primarily by twisting from a super-aligned CNT array synthesized via chemical vapor deposition (CVD) [38,39]. A schematic of the CVD process of the CNT array synthesis and the spinning process can be seen in Figure 7A,B. Our group developed and improved the synthesis process for spinnable CNT arrays and the related dry spinning and fiber post-treatment process. As a result,

high-purity CNT fibers were reproducibly fabricated and characterized, and the results are published elsewhere [40,41].

The recipe for spinnable arrays has been perfected over the years regarding the gas composition, flow rates, catalyst composition, reaction time, temperature, and pressure. The fibers that are produced have a large surface area. They are further post-treated to improve the mechanical and electrical properties [41–44]. The methods used to enhance mechanical strength and electrical conductivity practiced by our group were as follows:

- Performing fiber post-treatments such as (a) solvent densification, which decreases the cross-sectional fiber area, bringing the CNT bundles closer; and (b) post-spinning from a spun fiber (Figure 7C,D)
- Introducing optimized twisting during the spinning process;
- Annealing at a high temperature to remove the oxides and amorphous carbon and to increase the conductivity;
- Cross-linking of the CNTs fibers with appropriate polymers to increase their strength.

3.1.4. Twisting from CNT Films

This fiber fabrication method draws CNT fibers from thin CNT films and sheets via scrolling. During the scrolling, twisting, and drawing of the fibers, they are attracted to each other and self-align into a network of nanobundles with the help of van der Waal's interactions [45,46] Figure 8 illustrates the formation of biscrolling fibers with different types of twist insertions, such as Fermat-type, Archimedean-type, and dual Archimedean-type.

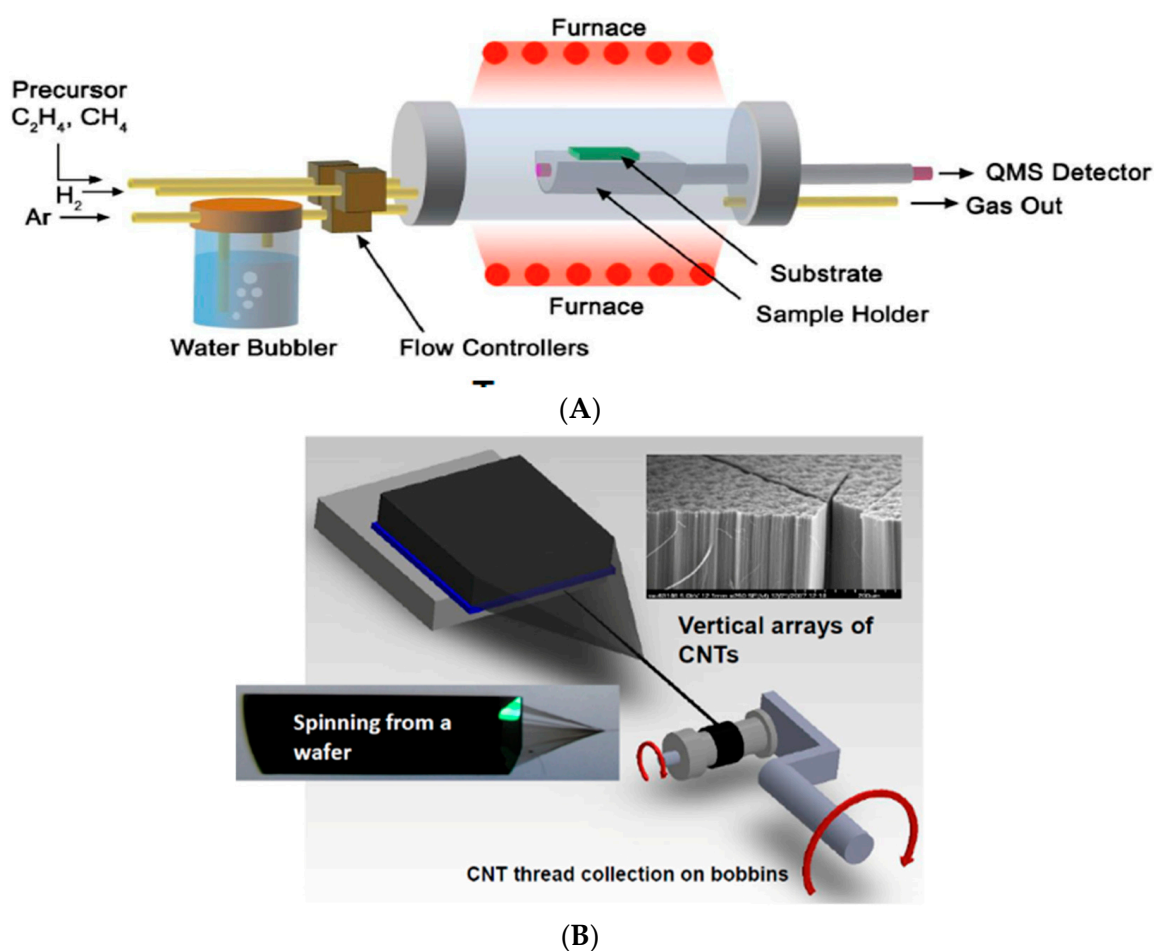


Figure 7. Cont.

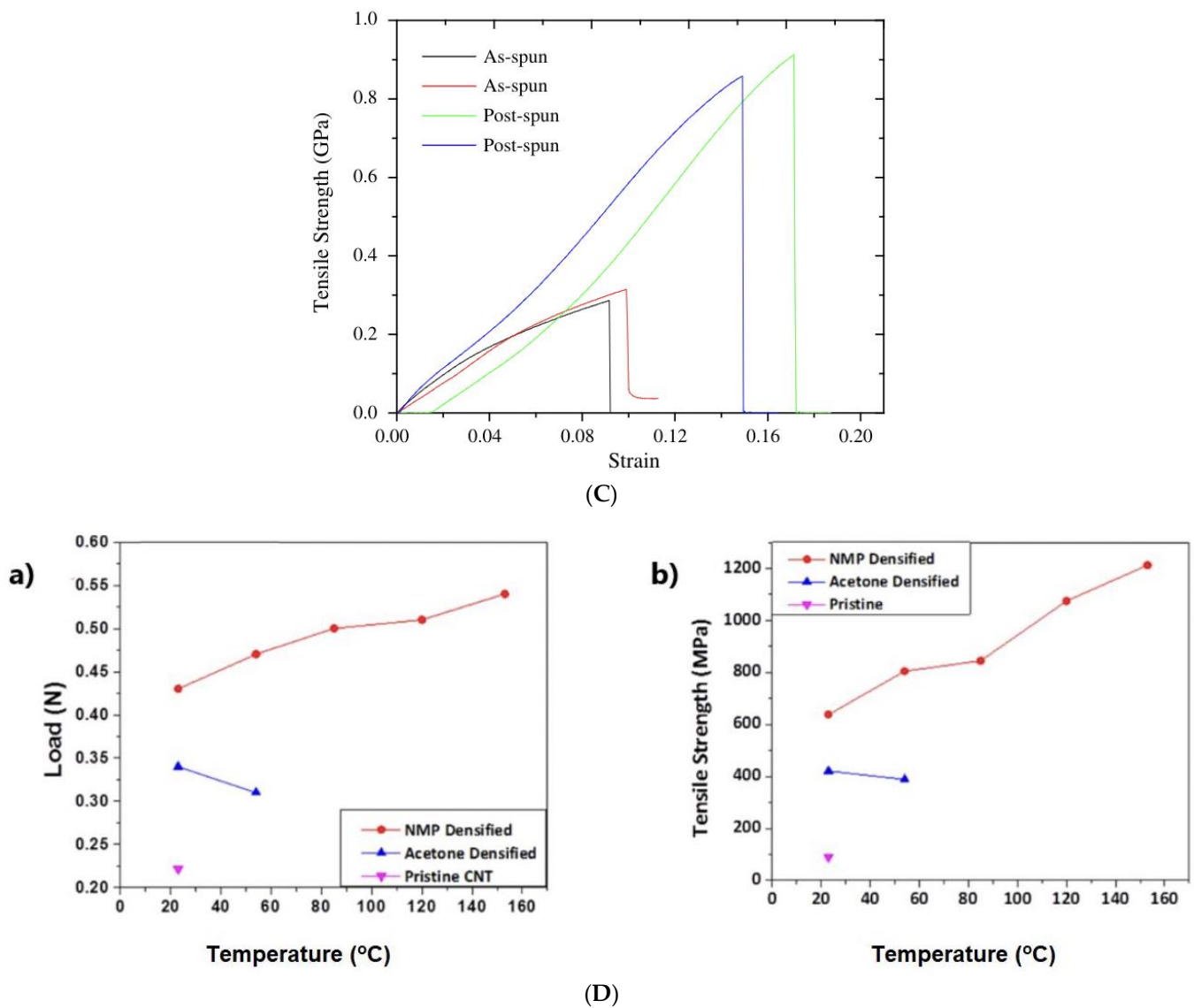


Figure 7. (A) Schematic of the thermal CVD process for the CNT array. (B) Schematic of the spinning of CNT fibers from the CNT forest array. (C) Schematic of as-spun fiber and post-spun fibers and comparison of the tensile strengths of “as-spun” and “post spun” CNT fibers. Reprinted with permission from [38] (D). Comparison of the mechanical (a) load-bearing and (b) tensile strengths of the pristine CNT fiber and the post-densified fiber with different solvents and temperatures. Reprinted with permission from [42].

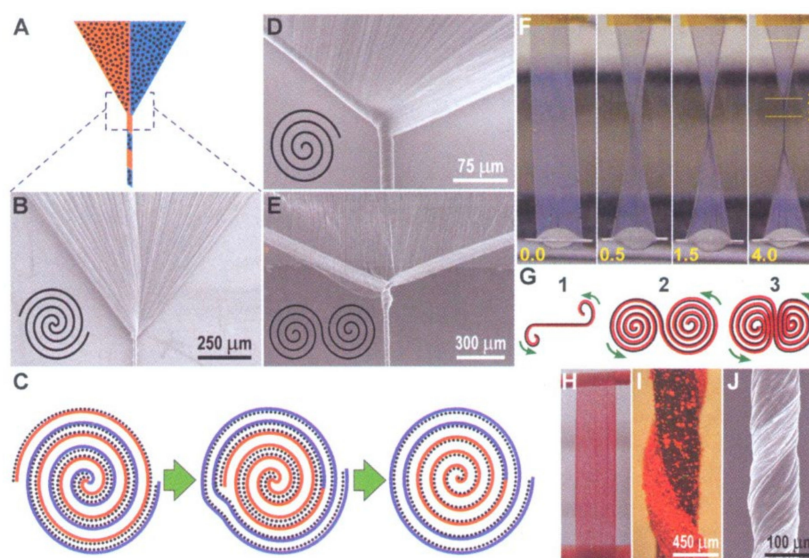


Figure 8. (A) Schematic of a twist induced in a CNT spinning web. The active loaded material is represented by black dots. (B) SEM image showing a Fermat-type twist (Fermat scroll shown in the inset). (C) Change from a Fermat to Archimedean scroll. (D) Archimedean scroll. (E) Dual Archimedean scroll. (F) Sequential pics of a liquid-state twist insertion in a multiwalled CNT(MWCNT) with filtration of the deposited boron nitride nanotubes. (G) Cross-sections of several twists marked in (F,H,I) pictures of actual MWCNTs colored with red paint, both unscrolled and scrolled. (J) SEM image of 70% Ti@MWCNT biscrolled yarn produced by symmetrically inserting a twist in a bilayer rectangular sheet supported in a liquid bath. Reprinted with permission from [45].

4. Strategies to Improve the CNT Fiber's Electrode Performance

As mentioned earlier, in CNTs, the only active material is carbon, so the available type of charge storage is a double layer. Double layers are insufficient for most practical applications due to their low capacitance and energy density. Hence, various strategies have been developed to improve the electrochemical performance of CNT electrodes, such as the (1) activating CNT fibers via heat treatment or surface oxidation to modify the surface properties and functionalities, (2) combining the CNT fiber with pseudocapacitive materials, and (3) co-plying with highly conductive metal wire [1,3,47,48].

4.1. Activation of CNT Fiber by Gamma Irradiation, Oxygen Plasma, or Acid Treatment

CNT fiber can undergo surface modifications via activation by gamma radiation, acids, and oxygen plasma. The treatments often lead to improvements in the electrochemical properties, which can be attributed to:

- The introduction of functional groups on the surface;
- The modification of the pore structure and the opening of new pores;
- Increasing the surface area;
- Decreasing the gravimetric density;
- Changing the surface energy by promoting hydrophilicity.

The effects mentioned above are reversed during the activation by heat treatment, with a decreased pore density and surface area, increased graphitization in the carbon microstructure, and increased gravimetric density [6].

4.1.1. Activation by Gamma Radiation

Su et al. [49] activated a CNT fiber using gamma irradiation and obtained improved mechanical, electrical, and electrochemical performances for two-ply yarn SCs. Significant improvements were seen in the mechanical strength (the breaking strength increased from 574.5 MPa to 773.4 MPa), conductivity (increased from $3596 \text{ S}\cdot\text{m}^{-1}$ to $5494 \text{ S}\cdot\text{m}^{-1}$), and

gravimetric capacitance (increased from $6.2 \text{ F}\cdot\text{g}^{-1}$ to $9.2 \text{ F}\cdot\text{g}^{-1}$) after irradiation. Additionally, the XPS results showed an increase in the percentage of O_2 from 0.4% to 3.6%.

4.1.2. Activation by Oxygen Plasma Treatment

Adusei et al. [50] studied the effects of atmospheric pressure oxygen plasma functionalization on CNT fibers. The CNT fibers were subjected to plasma functionalization for various plasma parameters, such as the plasma power and oxygen flow, characterized as (a) low (60 W and 0.1 L/min), (b) medium (100 W and 0.3 L/min), and (c) high (140 W and 0.55 L/min), respectively. The secondary gas (helium) flow rate was maintained at 15 L/min for all the other plasma parameters. The fibers were passed through the plasma head in a continuous roll-to-roll process at two linear speeds (0.465 cm/s and 0.206 cm/s). The electrochemical characterization of the treated CNT fibers under various conditions revealed that the medium-oxygen plasma-treated fibers (100 W and 0.55 L/min) with a lower speed of fiber passing through the plasma head (0.206 cm/s) gave the greatest specific capacitance. The treated fibers showed an increase in surface area from $168.22 \text{ m}^2/\text{g}$ to $208 \text{ m}^2/\text{g}$ and a 132.8% increase in specific capacitance. The impressive capacitance improvement was due to the introduction of functional groups on the CNT fiber containing oxygen, the increased hydrophilicity, and the enhanced surface area due to pore opening.

4.1.3. Activation by Acid Treatment

The acid treatment of CNT fibers after thermal oxidation was studied by Liang et al. [51]. First, the thermal oxidation of the iron nanoparticles formed during the tube growth was conducted in air at $400 \text{ }^\circ\text{C}$. Then, the acid treatment was performed by soaking the fiber in a mixture of $\text{HNO}_3\text{-H}_2\text{SO}_4$ (1:3 volume ratio) with stirring for 6 h, followed by rinsing with DI water and drying. As a result, the activated fiber showed an increase in oxygen level from 11.63% to 20.77%. In addition, the Brunauer, Emmett, and Teller (BET) surface area increased from $138.3 \text{ m}^2\cdot\text{g}^{-1}$ to $236.8 \text{ m}^2\cdot\text{g}^{-1}$. These two effects contributed to an outstanding electrochemical performance, achieving a capacitance rate of $1988 \text{ mF}\cdot\text{cm}^{-2}$ at $2 \text{ mA}\cdot\text{cm}^{-2}$ and cyclic stability of 10,000 cycles with only 3% capacitance loss.

4.2. Combining Pseudocapacitive Materials with CNT

Pseudocapacitive materials can combine redox reactions and double-layer charging to achieve higher capacitance rates and energy storage densities.

4.2.1. Deposition of Active Materials after Fiber Fabrication Metal Oxides and Hydroxides

MnO_2 is the most attractive pseudocapacitive oxide due to its low cost, abundance, and high specific capacitance value. However, it has the limitation of poor conductivity, and this problem imposes a great challenge, especially in highly loaded composites. Usually, introducing a nanoscopic scale of MnO_2 can provide adequate electrochemical performance, but low loading often causes low energy and power densities. Therefore, Kim et al. [52] found a solution to circumvent the conductivity issue while providing high loading with the oxide. They designed a composite electrode with CNT as the core layer with electrodepositing alternating layers of MnO_2 and Ag within the resulting sheath. The highly conductive intermediate silver layer shortened the ion diffusion length in the MnO_2 . In addition, it acted as a conductive bridge between MnO_2 aggregates and the Ag layer, so that during charging and discharging the flow of electrons is rapidly transferred by the Ag layer, which does not affect the rate capability of the device, irrespective of the amount of MnO_2 loading. The Ag/ MnO_2 parallel symmetric two-ply sheath-core yarn SC showed a capacitance of $322.2 \text{ mF}\cdot\text{cm}^{-2}$ ($208.1 \text{ F}\cdot\text{cm}^{-3}$) and an energy density of $18.3 \text{ }\mu\text{Wh}\cdot\text{cm}^{-2}$. The rate capability was increased from 21.2% to 42.6% from pristine MnO_2 sheath-core vs. Ag/ MnO_2 sheath-core SC.

As discussed earlier, the MnO_2 composite not only has the disadvantage of low conductivity but also a short cycle life. Zhou et al. [53] circumvented this problem by innovatively

adding black phosphorous into the CNT/MnO₂ composite. The CNT yarn was immersed in KMnO₄, HCl, and black phosphorous (BP) nanosheet aqueous solutions. The KMnO₄ was reduced to MnO₂, and the CNT/MnO₂/BP composite electrode was formed. Two polyvinyl alcohol (PVA)-KOH-coated CNT fibers were twisted into a two-ply yarn SC, which gave a promising electrochemical performance. The capacitance was reported to be 441.79 F·cm⁻³ at 0.01 V·s⁻¹. The energy density reached 9.82 mWh·cm⁻³, and the power density value was 441.79 mW·cm⁻³. This study also reported a 37.9-fold increase in capacitance for the CNT-MnO₂-BP yarn SC compared to the CNT yarn and a 2.4-fold increase compared to the CNT-MnO₂ yarn SC. According to the authors, these remarkable results can be attributed to the highly conductive CNT substrate, the pseudocapacitance provided by the MnO₂, and the rapid ion diffusion enabled by the phosphoric-acid-based electrolyte formed via the reaction of black phosphorous and KMnO₄ during the formation of MnO₂. The rapid ion diffusion helped to increase the specific capacitance and cyclic stability.

Zhou et al. [54] fabricated a sandwiched CNT composite by electrodepositing a pseudocapacitive transition metal oxide mixture of Co₃O₄@NiO and coating a graphene layer over it. The CNTs act as a substrate with a high specific surface area for the electrodeposition of the transition metal oxide, Co₃O₄@NiO, which offers numerous active sites for redox reactions. In addition, the graphene layer decreases the equivalent series resistance (ESR) and increases the power density and cycle life. A two-ply yarn SC was fabricated by twisting two composite sandwich fibers and applying PVA-KOH as an electrolyte between them. The SC yielded a high capacitance of 263 F·cm⁻³ at 0.01 V/s, an energy density of 5.86 mWh·cm⁻³, and a power density of 263.64 mW·cm⁻³.

Le et al. [55] introduced another innovative approach to improving the electrochemical performance using a two-step strategy, namely increasing the surface area by growing ZnO nanorods on the CNT surfaces and coating them with a pseudocapacitive material like a nickel cobalt double hydroxide. As a result, the electrode exhibited an excellent capacitance of 1278 F·g⁻¹ at a scan rate of 5 mV·s⁻¹ and cyclic stability of 7000 cycles with a capacity retention rate of 60.5%.

Metal Sulfides

Jian et al. [56] fabricated an SC, solving the issue of the delamination of metal oxides and sulfides coated on the CNT surfaces. For this, a hybrid substrate of CNTs and reduced graphene oxide (RGO) was prepared, where the RGO served as an adhesive layer. Molybdenum sulfide was then coated onto the hybrid layer to allow the pseudocapacitance. Thus, a composite electrode of MoS₂/RGO/CNT was formed. Next, a symmetric parallel SC was fabricated using PVA-H₂SO₄ as an electrolyte. The authors reported for this SC a capacitance of 190.4 F/g at 0.2 A·g⁻¹ and 85% capacitance retention after 5000 cycles.

4.2.2. Incorporation of Active Material before or during Fiber Fabrication

The deposition of active materials after the fiber formation has limitations because of the following reasons:

- Higher loading is not possible since it does not increase the capacitance, as the accessible surface area is considerably reduced;
- The resistance increases along with the ion diffusion distance, substantially reducing the power density, resulting in greater energy consumption.

As an alternative to surface deposition, embedding the active materials into the CNT structure before its formation seems to be a more practical approach. In this process, the nanosized active materials are overlaid on the CNT sheet or film before the fiber is twisted. Compared to surface cladding, this type of incorporation allows much higher loading and a closer contact of the active materials with the nanocarbon bundles, facilitating higher EDL pseudocapacitance. In addition, these materials can create more pores and channels for faster ion adsorption and diffusion, thereby increasing the capacitance, rate capability, and cyclic stability.

Shi et al. [57] successfully designed amorphous MnO₂@MWCNT fiber electrodes for SCs with improved flexibility, energy density, and high cyclic stability. Amorphous MnO₂, which has a highly disordered structure, was incorporated into the MWCNT sheet by immersing a stacked MWCNT sheet into a mixture of a KMnO₄/H₂SO₄ aqueous solution, followed by twisting the sheets into a fiber with the help of an electric motor. Two such twisted yarns were used to fabricate symmetric solid-state SCs using PVA-LiCl as an electrolyte, which showed a capacitance of 8.5 F·cm⁻³ (13-fold than MWCNT fiber SC) and an energy density of 1.5 mWh·cm⁻³, and surpassed 15,000 charge–discharge cycles retaining 90% of the capacitance. Furthermore, due to the close contact between the MnO₂ and MWCNT, the synergy between them made the highly aligned MWCNT substrate with uniformly distributed MnO₂ particles highly conductive and mechanically stable. Additionally, the nano MnO₂ particles with large surface areas provided numerous accessible active sites for redox reactions, shortening the electron and ion diffusion lengths and allowing the MnO₂ to be accessible for charge storage.

5. Strategies to Improve Device Performance

As mentioned in Section 2.3, a supercapacitor device is assessed by its energy density and power density.

The energy density is given by Equation (3):

$$E = \frac{1}{2}CU^2$$

and the power density is given by Equation (4)

$$P = \frac{U^2}{4R_s}$$

where U is the working voltage, C is the capacitance, and R_s is the internal resistance.

Increasing the working voltage is more impactful than increasing the capacitance to raise the energy density. The working voltage can be increased by:

- Configuring an asymmetric type of capacitor;
- Using electrolytes with a wide working voltage;
- Modifying the electrode to widen the voltage window;
- Using redox electrolytes.

To increase the power density, the internal resistance has to be reduced by increasing the conductivity. One way to increase the conductivity is via co-plying with metals [1,58].

5.1. Metal Wire Co-Plying

CNT fiber SCs, because of their increased length, will have high internal resistance, resulting in a large potential drop under a high current density. To improve the rate capabilities at higher currents, it is often helpful to couple a highly conductive metal wire with CNTs for fast electron transfer.

Wang et al. [59] fabricated (Figure 9A) an SC with individual electrodes consisting of CNT and Pt yarn twisted together at 5000 turns/min and coated with PANI. The yarn was named Pt/CNT@PANI. When subjected to cyclic voltammetry at a very high scan rate of 500 mV/s, the symmetric SC maintained a symmetrical shape compared with those formed at 10 mV/s. Figure 9(Bb) displays the capacitance–voltage (CV) curves at 100 mV/s for a PANI-coated CNT fiber with and without platinum. Additionally, a galvanostatic charge–discharge (GCD) test was conducted. The CV and GCD curves showed that the SC with platinum provided a greater capacitance area in the CV curve and a longer discharge time in the GCD test. Figure 9C shows the rate capability result, highlighting that a capacitance retention rate of 68% was achieved when the current density was increased from 0.8 to 40 mA·cm⁻², revealing good stability over large currents. The electrochemical impedance spectroscopy (EIS) measurements with a frequency loop from 10⁵ Hz to 10² Hz using an

amplitude of 5 mV at an open-circuit potential (Figure 9(Bf)) showed that the SC with Pt gave an ESR of 30 ohms.

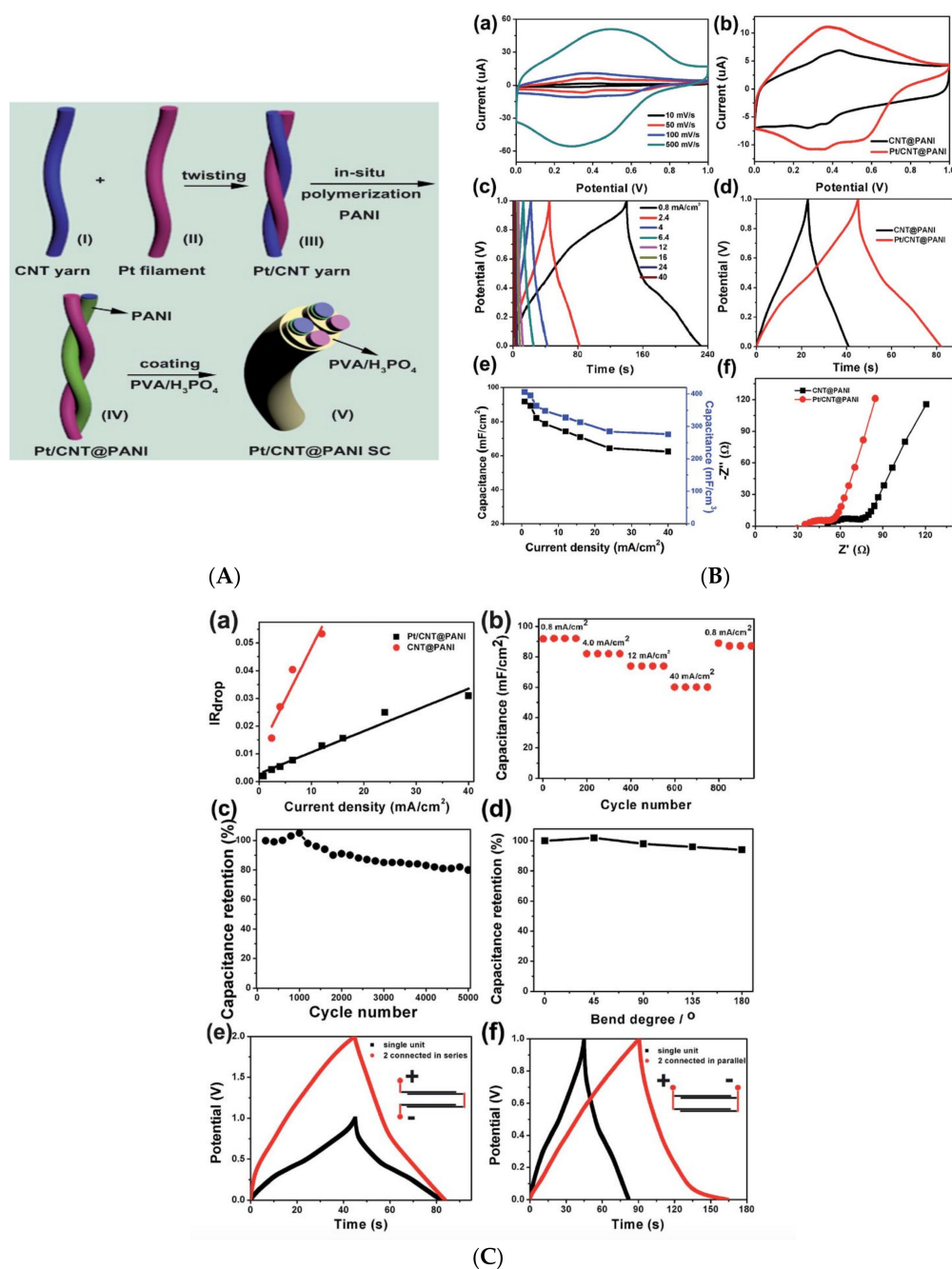


Figure 9. (A) Schematic of the fabrication of SCs. (B) The electrochemical properties of two-ply nanocomposite yarn SCs: (a) CV of the Pt/CNT@PANI yarn SC; (b) CV curves of CNT@PANI and Pt/CNT@PANI yarn SCs at $100 \text{ mV} \cdot \text{s}^{-1}$; (c) galvanostatic charge–discharge (GCD) curves of the Pt/CNT@PANI yarn SC at different current densities; (d) GCD curves of CNT@PANI and Pt/CNT@PANI SCs at $2.4 \text{ mA}/\text{cm}^2$; (e) areal capacitance of the Pt/CNT@PANI yarn SC at different current densities; (f) EIS of CNT@PANI and Pt/CNT@PANI SC devices. (C) Characterization of the Pt/CNT@PANI nanocomposite yarn supercapacitor: (a) IR loss (drop of the cell internal resistance) as a function of the discharge current density; (b) cycle performance at varying current densities; (c) capacitance retention with different charging–discharging cycles and a constant current density of $4 \text{ mA}/\text{cm}^2$; (d) capacitance retention under different bending states; (e) GCD of two devices connected in series and (f) in parallel. Reproduced with permission from [59].

In contrast, without Pt, this parameter result was 40 ohms. The IR drop against the increasing current gave a smaller value and a less steep slope for the SC with Pt compared to the one without Pt. The SC with Pt also exhibited good cyclic stability with a capacitance retention rate of 80% after 5000 cycles. The PANI-coated CNT SC with Pt yielded a capacitance rate of $91.67 \text{ mF}\cdot\text{cm}^{-2}$, an energy density of $12.68 \text{ }\mu\text{Wh}\cdot\text{cm}^{-2}$, and good cyclic stability.

Wu et al. [60] also twisted a number of CNT yarns with a platinum wire followed by PANI deposition. The 5 CNT yarns twisted with Pt gave the best results. Notably, Pt/5-CNT@PANI showed excellent electrochemical performance, revealing a specific capacitance rate of $217.7 \text{ F}\cdot\text{g}^{-1}$ at 0.2 A/g current density, an energy density of 30.22 Wh/kg , and a power density of 91.88 W/kg .

Wang et al. [61] reported on copper wire intertwined with CNT to be used as a current collector. The spinel-type nickel–cobalt oxide was hydrothermally deposited on the obtained composite yarn. According to these authors, the SC was fabricated from two individual CNT/copper intertwined yarns on which NiCo_2O_4 (NCO) nanowires were grown. The Cu enhances the conductivity, and the porous CNT allows quick charge transport between the electrolyte and the electrode. NCO was the only electroactive material used. The obtained SC exhibited a capacitance of $277.3 \text{ mF}\cdot\text{cm}^{-2}$ and an energy density of $35.76 \text{ }\mu\text{Wh}\cdot\text{cm}^{-2}$ at a power density of $0.154 \text{ mW}\cdot\text{cm}^{-2}$. In addition, this device showed excellent cyclic stability, with 89% capacitance retention after 5000 cycles.

5.2. Fabrication of an Asymmetric-Type Configuration

Symmetric SCs consist of positive and negative electrodes of the same active material with the same weight. The working voltage of a symmetric SC depends on the electrolyte and the active materials' potential window (PW). The PW is limited when an aqueous electrolyte is used due to water electrolysis (1.23 V (thermodynamic value), resulting in hydrogen and oxygen evolution. For pseudocapacitive materials such as PANI, PPY, and MnO_2 , the PW can be narrower as the PW of the electrolyte can impact it. Additionally, the specific capacitance of a two-electrode SC made of pseudocapacitive materials such as PANI and PPY is always inferior to those obtained using three electrodes, because in a two-electrode cell the positive and negative electrodes will be working in different potentials, leading to different specific capacitances. This means that the one with the lower capacitance will determine the total specific capacitance, as per the Equation (2)

$$\frac{1}{C} = \frac{1}{C_1} + \frac{1}{C_2}$$

The performance matrix of an SC, like the energy and power density, can be increased by raising the working voltage, which can be expanded by using an asymmetric configuration. This can be achieved via different active materials at the positive and negative electrodes with different PWs, or when using the same active material with varying mass ratios. The PW can be wider if the positive electrode is reversibly charged to a maximum high and the negative one to a low minimum value. An asymmetric capacitor can give a maximum capacitance when $C_1 = C_2$, or $\text{CM}_+\text{M}_+ = \text{CM}_-\text{M}_-$, where CM_+ , M_+ , CM_- , and M_- are the gravimetric capacitance and mass ratios of the positive and negative electrodes, respectively. Asymmetric SCs can be fabricated from a host of positive and negative electrodes and can have wider working voltages and capacitances, resulting in very high energy and power densities [3,4]. The common pseudocapacitive materials and their properties are listed in Tables 1 and 2 of Section 2.1.

5.2.1. Transition Metal Oxide and Hydroxide Based Asymmetric Capacitors

Most asymmetric SCs reported in the literature are fabricated using transition metal oxides, hydroxides, sulfides, and nitrides (Ni, Co, Fe, V, Ti, Mo) as the pseudocapacitive materials. Yao's group [62] investigated the growth of Co_3O_4 on conductive substrates such CNT fibers. They used these for a positive electrode when fabricating an SC with

vanadium nitride nanowires grown on the CNTs as the negative electrode. Co_3O_4 is an inexpensive and promising positive electrode material with high theoretical capacitance. Vanadium nitride, employed as a negative electrode, has a very high theoretical capacitance of 1340 F. A PVA-KOH gel electrolyte was used, which provided a cell voltage of 1.6 V. The SC exhibited an energy density of $15.79 \text{ mWh}\cdot\text{cm}^{-3}$ and a power density of $3.232 \text{ W}\cdot\text{cm}^{-3}$. The SC gave a capacity retention rate of 93.01% after 3000 bend cycles at 90° .

Layered transition metals hydroxides (TMOH) such as $\text{Ni}(\text{OH})_2$ and $\text{FeO}(\text{OH})$ are capable of fast redox reactions within the space between the layers, thereby increasing the capacitance value.

Lu's group [63] constructed a coaxial type of SC to ward off the decreased specific capacitance effects with parallel and twisted construction types and successfully fabricated an SC with $\text{MoS}_2@ \text{Fe}_2\text{O}_3/\text{CNT}$ paper as the negative electrode and $\text{Ni}(\text{OH})_2 @ \text{NiCo}_2\text{O}_4/\text{CNT}$ fiber as the positive electrode with a PVA-KOH electrolyte. With a voltage window of 1.6 V, the SC gave a specific capacitance of $373 \text{ F}\cdot\text{cm}^{-2}$ at a current density of $2 \text{ mA}\cdot\text{cm}^{-2}$. The achieved energy density was $0.13 \text{ mWh}\cdot\text{cm}^{-2}$, the power density $3.2 \text{ mW}\cdot\text{cm}^{-2}$, and the capacity retention rate was 83.3% after 10,000 cycles.

Various combinations of positive and negative electrodes were attempted, with the researchers claiming higher working voltages. However, the obtained energy density values are still unsatisfactory for practical applications.

Yao's group [64] successfully fabricated a ternary metal oxide (ZnNiCo) with nickel hydroxide nanowire arrays (NWAs), cladding the CNT fiber as the positive electrode ($\text{ZnCo}@ \text{Ni}(\text{OH})_2 \text{NWAs}/\text{CNTF}/\text{KOH-PVA}$) and a thin layer of carbon coated vanadium nitride on the CNT fiber as the negative electrode ($\text{VN}@ \text{C NWAs}/\text{CNTS}$) in a coaxial fiber configuration (Figure 10A). The coaxial fiber-based asymmetrical supercapacitor (CFASC) gave an impressive specific capacitance of $94.67 \text{ F}\cdot\text{cm}^{-3}$, with an energy density of $33.66 \text{ mWh}\cdot\text{cm}^{-3}$ and with more than 90% capacitance retention after 3000 bend cycles (Figure 10B). Other transition metal oxide (TMO)-based asymmetric capacitors are displayed in Table 4.

Yao's group [65] fabricated a fiber supercapacitor (FSC) with a ternary oxide (MoNiCo) on CNT fiber as the positive electrode and thin carbon-coated vanadium nitride nanowires on CNT fiber as the negative electrode with PVA-KOH as the gel electrolyte. The use of a ternary oxide is intended to increase the electronic conductivity and electrochemical activity due to the mixed valence metal cation. This might not be the case when mono- or bi-metal oxides such as Co_3O_4 are used, which suffer from low capacitance and electrical conductivity levels. Furthermore, the hierarchical dandelion-like ternary oxide structure on the CNTs provides a greater surface area, leading to more accessible sites on the electrode for the electrolyte, resulting in fast electron ion transport. The authors of this work reported an SC with a voltage window of 1.6 V, capacitance of $62.3 \text{ F}\cdot\text{cm}^{-3}$, energy density of $22.2 \text{ mWh}\cdot\text{cm}^{-3}$, and 90.2% capacitance retention after 3500 bend cycles.

Peng's group [66] fabricated an FSC using a polyimide-based polymer for high mechanical strength and MnO_2 for high pseudocapacitance. As a result, the FSC revealed a reasonably high working voltage of 2.1 V, mechanical strength of 264 MPa (tensile strength), energy density of $36.4 \mu\text{Wh}\cdot\text{cm}^{-2}$, and power density of $0.78 \text{ mW}\cdot\text{cm}^{-2}$. These results are credited to the combination of MnO_2/CNT as the positive electrode and polyimide/CNT as the negative electrode with carboxy methyl cellulose (CMC)/ Na_2SO_4 as the electrolyte in a parallel configuration with a voltage window of 2.1 V.

Zhang's group [67] successfully investigated the pre-insertion of cations such as Na^+ onto MnO_2 nanosheets to enhance the capacitance (Figure 11A).

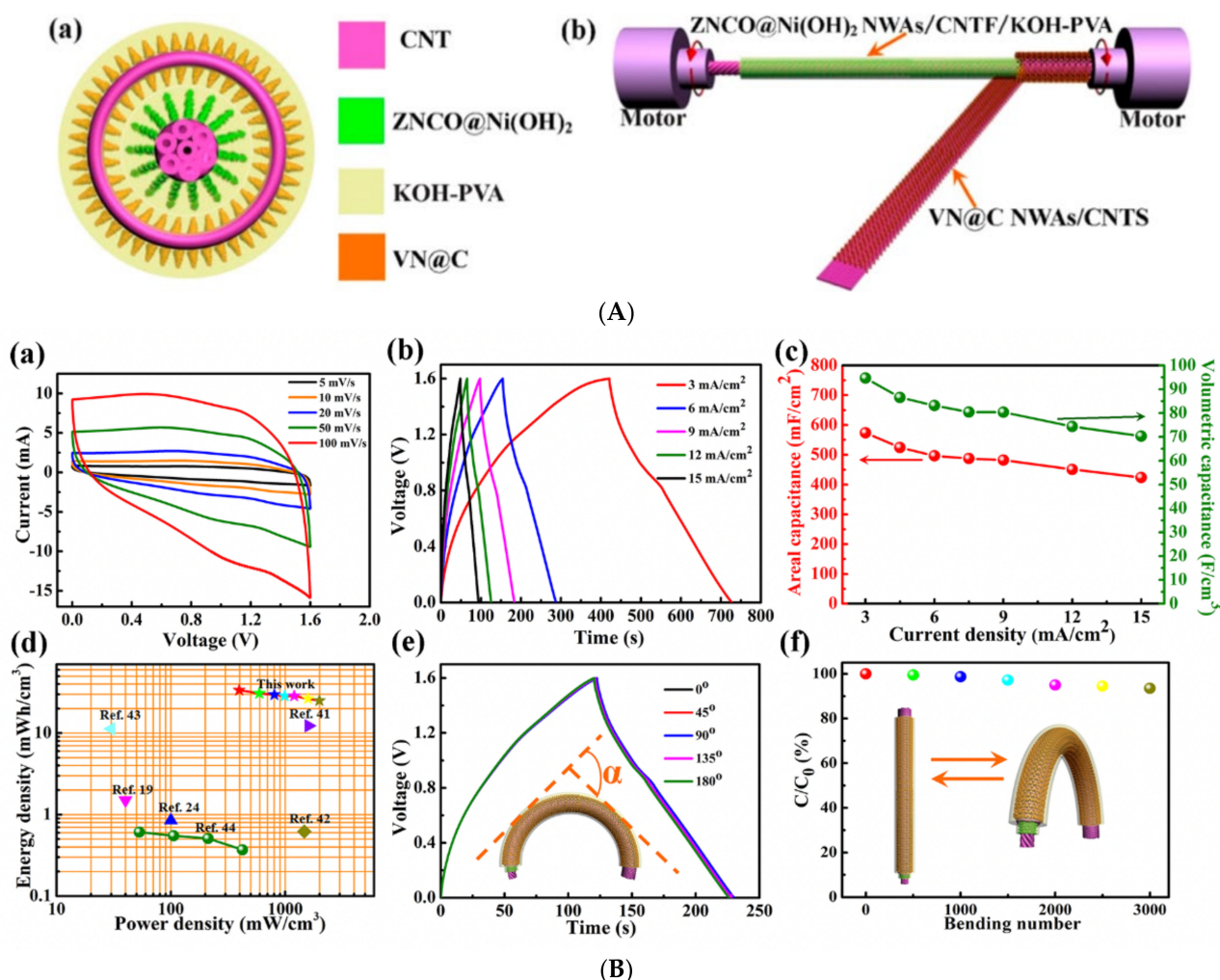


Figure 10. (A) (a) Cross sectional structure of the CFASCs (coaxial fiber shaped asymmetric supercapacitors). (b) Wrapping of the VN@C NWs/CNTs around the surface of the ZNCO@Ni(OH)₂ NWs/CNTF/KOH-PVA. (B) Electrochemical characterization and flexibility analysis of the as-assembled CFASCs: (a) CV curves of the assembled CFASCs measured at different scan rates between 0 and 1.6 V; (b) GCD curves collected at different current densities between 0 and 1.6 V; (c) areal and volumetric specific capacitances calculated from the GCD curves as a function of the current density; (d) volumetric energy and power densities of CFASCs compared with previously reported FASCs (fiber shaped asymmetric supercapacitors); (e) GCD curves of the as-assembled CFASCs bent at various angles and a current density of 10 mA/cm²; (f) Normalized capacitances of our CFASCs bent 90° for 3000 cycles. Reproduced with permission from [64].

The low conductivity of MnO₂ results in poor ion diffusion, and the insertion of Na/K ions improves the conductivity, thereby enhancing the capacitance. An FSC with a twisted configuration, as shown in Figure 11A, showed good performance due to the effective design of the positive electrodes as Na-doped thin MnO₂ nanosheets on the CNT fiber. The adequately chosen negative electrode, which was a flowerlike thin MoS₂ nanosheet array, provided the SC with a high working voltage of 2.2 V. As reported in this publication, the FSC exhibited a high specific capacitance of 265.4 mF·cm⁻² and energy density of 178.4 μWh·cm⁻². Moreover, no capacitance loss was noticed after 3500 bending cycles at 120° (Figure 11(Bf)).

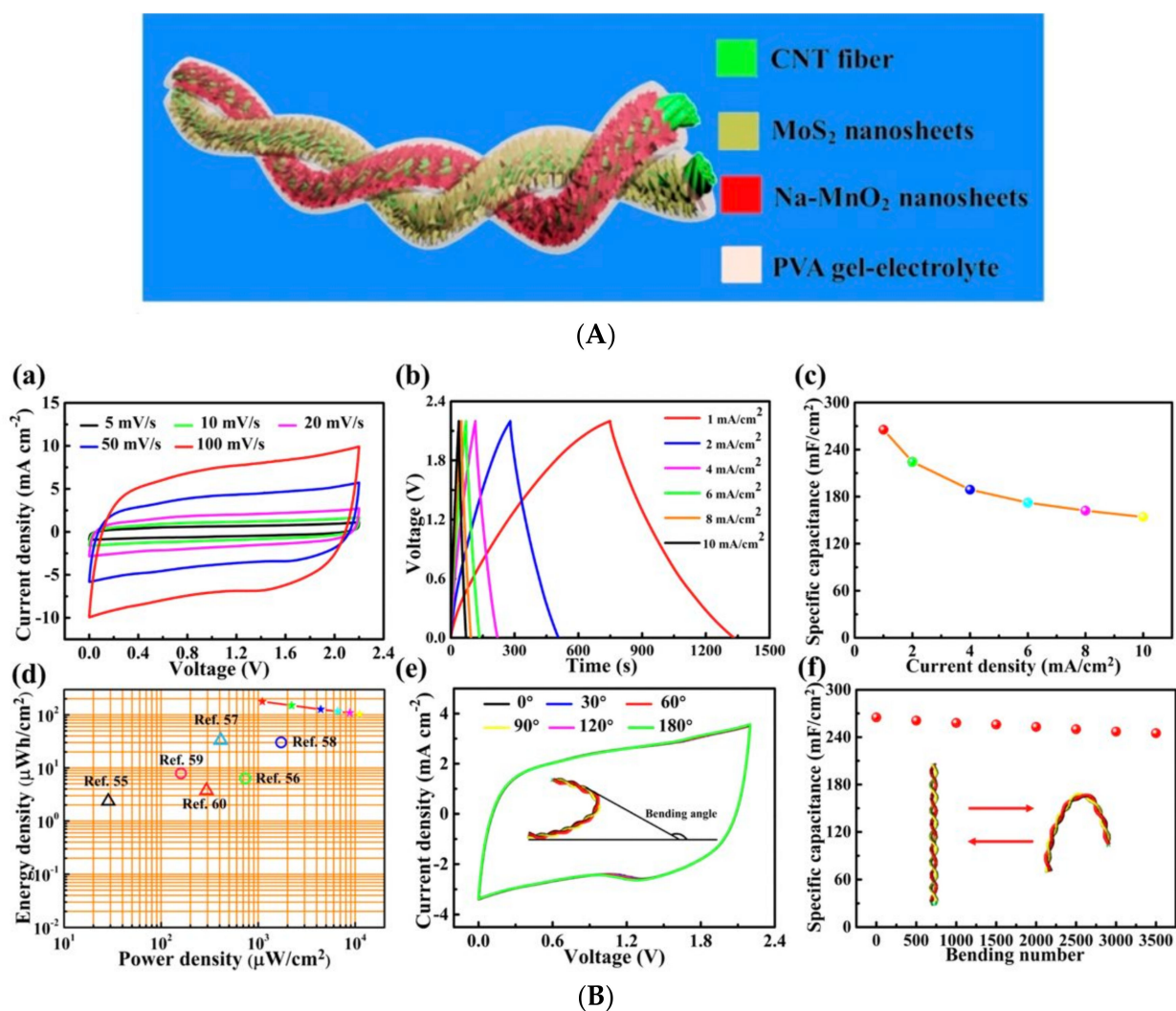


Figure 11. (A) Detailed illustration of the fiber shaped asymmetric supercapacitors (FASCs) (B) Electrochemical study of the FASCs: (a) FASC CV curves at various scanning rates of 5–100 mV/s; (b) GCD curves with different current densities of 1–10 mA/cm²; (c) areal specific capacitance as a function of the current density; (d) FASC power density and areal energy density compared to previous FSCs; (e) CV curves of the FASCs under various bending angles; (f) capacitance retention of the FASCs exposed to bending angles of 120° for 3500 cycles. Reproduced with permission from [67].

5.2.2. Conducting Polymer-Based Asymmetric Supercapacitors

Chen's group [68] developed an easy synthesis technique wherein a mixture of CNTs plus PPY is deposited on the CNT core (positive electrode), and a mixture of RGO plus CNTs is electrodeposited on the CNT core as the negative electrode (Figure 12A). The created fiber shaped asymmetric SC (FASC) gave a higher specific capacitance and greater mechanical strength. The gel electrolyte PVA-H₃PO₄ provided a voltage of 1.6 V, which yielded a capacitance of 58.82 mF·cm⁻². The FSC (fiber-based SC) was fabricated as illustrated in Figure 12A, and the hierarchical construction resulted in a 3D pore structure providing a better electrochemical performance. The authors reported an energy density of 20.91 μWh·cm⁻² and a power density of 6.4 mW·cm⁻². The specific capacitance retention rate was 98.6% after 200 bend cycles and 90% after 10k regular charge–discharge cycles (Figure 12C).

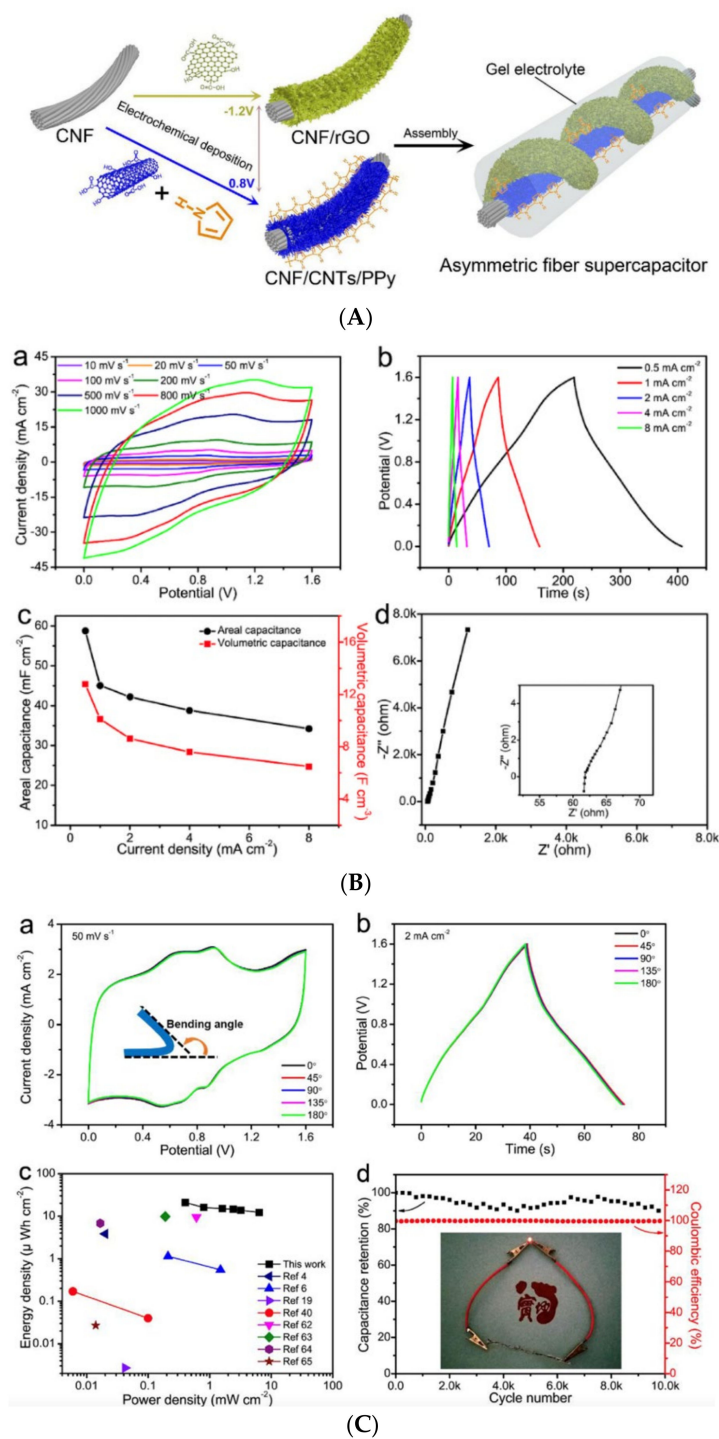


Figure 12. (A) Schematic of the fabrication of an FASC. (B) Electrochemical performances of FASC: (a) CV curves at various scan rates ranging from 10 to $1000\text{ mV}\cdot\text{s}^{-1}$; (b) GCD curves at the current densities from 0.5 to $8\text{ mA}\cdot\text{cm}^{-2}$; (c) areal and volumetric specific capacitances at various current densities; (d) Nyquist plots carried out in a frequency range from 100 kHz to 10 MHz. The inset shows the enlarged plot in the high-frequency region (C): (a) CV curves for the asymmetric capacitor at a scan rate of $50\text{ mV}\cdot\text{s}^{-1}$, under different bending states, with the inset showing an illustration of an asymmetric supercapacitor at different bending angles; (b) GCD curves at a current density of $2\text{ mA}\cdot\text{cm}^{-2}$ for the asymmetric supercapacitor under different bending states; (c) Ragone plots of the presently and previously reported supercapacitors; (d) capacitance retention during 10,000 GCD cycles. The inset shows a LED lit up at 2.4 V by two asymmetric supercapacitors in series. Reprinted with permission from [68].

Table 4 summarizes the current asymmetric SCs reported recently with details about their configuration, electrodes, electrolyte, working voltage, and electrochemical performance.

5.3. Use of Electrolytes with a Wide Potential Window

Electrolytes with a wide potential window can increase the working voltage to improve the device's performance. The most commonly used electrolytes in SCs are aqueous solutions based on sodium sulfate (Na_2SO_4), potassium hydroxide (KOH), and sulfuric acid (H_2SO_4). These have the following advantages:

- High ionic conductivity;
- Environmental benignity;
- Non-flammability;
- Small ionic radius.

However, their PW is limited to 1.23 V due to the earlier mentioned reasons. Another option is to use organic electrolytes with a greater potential window of 2.5–3 V. Nevertheless, organic solvents are flammable, volatile, toxic, and unsafe. Additionally, the power density could be poor due to the low conductivity of the organic electrolytes. Another group of non-volatile electrolytes is ionic electrolytes, which are less flammable with a PW greater than 3. Therefore, it is the safest group among the above three. Gel polymer electrolytes represent a recent group of electrolytes that are used widely for solid-state SCs. They are made by mixing a polymer with an ionic or organic electrolyte and can provide a wide voltage window that ensures good performance [3]. For example, Shanov's group [50] compared the specific capacitance of an oxygen-plasma-functionalized CNT fiber SC in three electrolytes. The SC with the PVDF-EMIMBF₄ electrolyte gave 25% and 65% more capacitance than the PVDF-EMIMTFSI and PVA-H₂SO₄ electrolytes, respectively.

Table 4. Summary of the asymmetric supercapacitors and their characteristics recently reported in the literature.

Electrodes							
Positive	Negative	Electrolyte, Cell Voltage	Capacitance	Energy Density (Ed)	Power Density (Pd)	Capacity Retention/No. of Cycles	Ref
NCO/VG@CNTF	VG@CNTF	PVA-KOH (1.8 V)	188 F·g ⁻¹ @ 5 A·g ⁻¹	65 Wh·kg ⁻¹	100 W·kg ⁻¹	93.1% after 5k bending cycles	[69]
PANI-CNTF	FeC ₂ O ₄ /FeOOH-CNTF	PVA-KOH (2.1 V) PVDF-EMIMBF ₄ (2.8 V)	-	0.05–4.07 μWh·cm ⁻² 0.17–3.06 μWh·cm ⁻²	0.18–0.92 μW·cm ⁻² 0.26–0.97 mW·cm ⁻²	96.76% of Ed retention after 4k bending cycles	[70]
PEDOT: PSS	CNTF	Chitosan (1.4 V)	21.4 F·g ⁻¹	5.83 Wh·kg ⁻¹	1399 W·kg ⁻¹	90% after 200 bending cycles	[71]
NiCo ₂ S ₄ @CNTF	VN@CNTF	PVA-LiCl (1.6 V)	86.2 F·cm ⁻³ @ 0.1 mA·cm ⁻³	30.64 mWh·cm ⁻³	80 mW·cm ⁻³	91.94% after 5000 bending cycles	[72]
CNTF/Porous CNT/PPY	CNTF/RGO	PVA-H ₃ PO ₄ (1.6 V)	58.82 mF·cm ⁻² (12.8 F·cm ⁻³)	20.91 μWh·cm ⁻²	6.4 mW·cm ⁻²	98.6% after 200 bend cycles, 90% after 10k cycles	[68]
GCF@NC@NCO	P-GCF	PVA-KOH (1.55 V)	33.6 mF·cm ⁻² @ 0.61 mA·cm ⁻²	11.2 μWh·cm ⁻²	472.1 μW·cm ⁻²	93% after 10k cycles	[73]
N doped CNT on CNT/LTO	N doped CNT on CNT	LiPF ₆ (in 1:1 EC/DEC) (2.5 V)	-	0.296 mWh·cm ⁻²	0.172 mW·cm ⁻²	100% after 4k cycles	[74]
CNT@PPY	CNT@CuCo ₂ O ₄	PVA-KOH (1.6 V)	59.55 mF·cm ⁻²	20 μWh·cm ⁻²	5.115 mW·cm ⁻²	80.1% after 8k cycles	[75]
VO ₂ @PPY/CNT	VN@NC/CNT	PVA-LiCl (1.8 V)	60.6 F·cm ⁻³	27.3 mWh·cm ⁻³	225 mW·cm ⁻³	88.9% after 4k bending cycles	[76]
Ni(OH) ₂ @NiCo ₂ O ₄ /CNTF	MoS ₂ @Fe ₂ O ₃ /CNTpaper	PVA-KOH (1.6 V)	373 F·cm ⁻² @ 2 mA·cm ⁻²	0.13 mWh·cm ⁻²	3.2 mW·cm ⁻²	80.3% after 2k cycles @ 20mAcm ⁻²	[63]

Table 4. Cont.

Electrodes							
Positive	Negative	Electrolyte, Cell Voltage	Capacitance	Energy Density (Ed)	Power Density (Pd)	Capacity Retention/No. of Cycles	Ref
ZNCO@Ni(OH) ₂ NWAs/CNTF	VN@C NWAs/CNTF	PVA-KOH (1.6 V)	94.67 F·cm ⁻³ @3 mA·cm ⁻²	33.66 mWh·cm ⁻³	396 mW·cm ⁻³	93.6% after 3k bending cycles at 90°	[64]
Co ₃ O ₄ NWAs/CNTF	VN (NWA)/CNTF	PVA-KOH (1.6 V)	44.4 F·cm ⁻³ @0.4 A·cm ⁻³	15.79 mWh·cm ⁻³	3.232 W·cm ⁻³	93.12% after 4k cycles 93.01% after 3k bending cycles	[62]
MNCO/CNTF	VN@C(NWA)/ CNTF	PVA-KOH (1.6 V)	62.3 F·cm ⁻³ @1 mA·cm ⁻²	22.2 mWh·cm ⁻³	213.3 mW·cm ⁻³	90.2% after 3.5k bending cycles	[65]
ZNCO NWA/CNTF	VN/CNTF	PVA-KOH (1.6 V)	50.0 F·cm ⁻³ @0.1 A·cm ⁻³	17.78 mWh·cm ⁻³	80.0 mW·cm ⁻³	91.0% after 3K bending cycles at 90°	[77]
Ti@TiO ₂	CNTF	PVA-H ₃ PO ₄ (1.4 V)	-	11.7 Wh·kg ⁻¹	2060.0 W·kg ⁻¹	91.0% after 1.2k bending cycles	[78]
CNT/MnO ₂	CF/PPY	LiCl-PVA (1.6 V)	66.27 mF·cm ⁻²	23.56 μWh·cm ⁻²	-	83% after 5k cycles	[79]
MnO ₂ /CNT	PI/CNT	CMC/Na ₂ SO ₄ (2.1 V)	59.2 mF·cm ⁻² @0.74 mA·cm ⁻²	36.4 μWh·cm ⁻² 30.2 μWh·cm ⁻²	0.78 mW·cm ⁻² 15.6 mW·cm ⁻²	96.3% after 2k cycles	[66]
Na- MnO ₂ @CNTF	MoS ₂ @CNTF	PVA/Na ₂ SO ₄ (2.2 V)	265.4 mF·cm ⁻² @1 mA·cm ⁻²	178.4 μWh·cm ⁻²	1100.9 μW·cm ⁻²	90% after 5k cycles	[67]

6. Stretchability of Wearable Supercapacitors

One of the most critical and emerging requirements of wearable fiber-based energy storage devices is the stretchability. In addition to other criteria for these devices such as the safety, bendability, low gravimetric density, and durability, an important one factor is the undeterred electrochemical properties during the deformations caused by the user's movements. An evaluation metric for the feasibility of such devices is their ability to withstand the frequency of human motion, including small- and large-scale motions falling in the frequency range of 0.1 and 10 Hz. At a minimum, such devices need to tolerate strains of 100% [80]. This section summarizes the advancements in developing CNT fiber supercapacitors by prioritizing the mechanical properties that can withstand high torsional strains and bending, while maintaining high capacitance retention rates.

Several variations in the manufacturing process impact the CNT fiber supercapacitor's mechanical and electrochemical properties. As already mentioned, adding pseudocapacitive materials such as metal oxides or organic polymers can improve the individual fibers' electrochemical properties. The electrodeposition of MnO₂, PANI, RuO₂, and Au have all been investigated. The results of their mechanical testing are presented in Table 5, which is displayed later. The tradeoff between using metal oxides and organic polymers is the material cost and the added weight to the fibers. Metals at optimal concentration contribute a substantial portion to the total weight of the fibers. The varying configurations all utilized different pseudocapacitive materials and were adopted to test the mechanical properties of the fibers in different ways, making it difficult to draw direct comparisons from the information available in the public domain.

6.1. Physical Configurations

6.1.1. Buckled CNT Sheets with an Elastomer Core

Buckling CNT sheets around an elastomer core are manufactured for creating individual stretchable electrodes utilized in supercapacitors. Their fabrication method includes stretching an elastomer core and wrapping a single or several CNT sheets around the elastomer. When the elastomer is relaxed, the CNT sheet buckles, as depicted in Figure 13, which enables a high surface area to be in contact with the fiber [81].

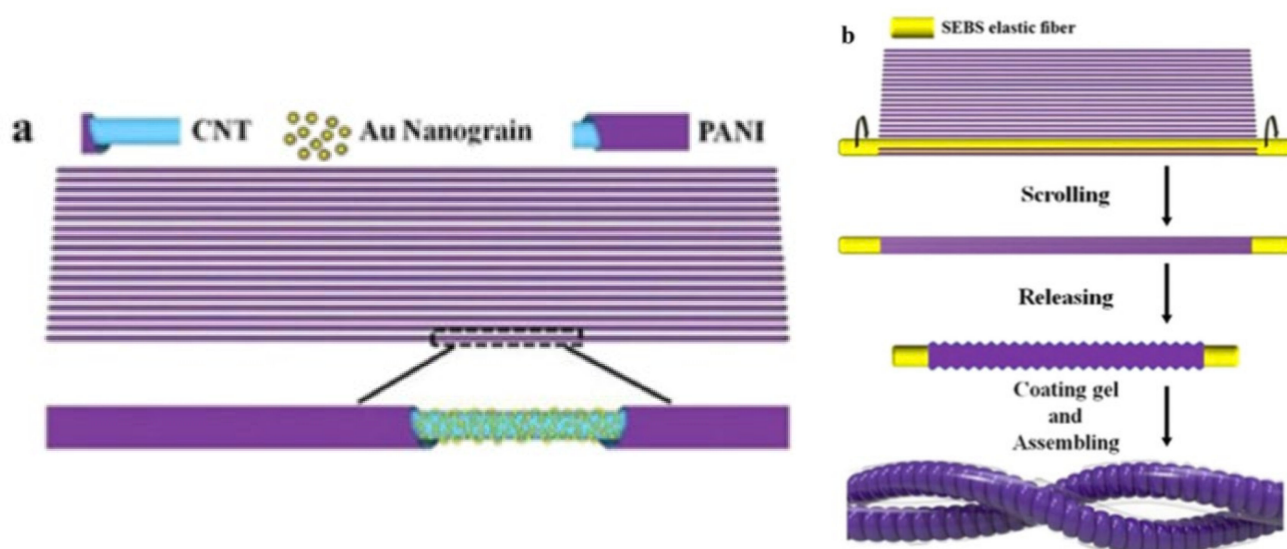


Figure 13. Schematic of the fabrication process of a stretchable linear elastomer-based FSC. (a) fabrication of the PANI@Au_x@CNT electrode, where 'x' represents the deposition time of Au nanoparticles. PANI was electrodeposited onto Au_x@CNT sheets. (b) Stretching of elastic fiber, wrapping of the electrodes, and twisting to fabricate the SC. Reprinted with permission from [81].

The buckling pattern is one of the topologically effective patterns used to save space for an otherwise stretchable and lengthy fiber capacitor, which helps to meet one of the most desirable requirements in wearable devices. The densification is often used to adhere the CNT sheets to the elastomer. The latter does not improve the electrochemical properties of the devices and adds additional weight and the benefit of enhanced mechanical properties. Many elastomers have been utilized across the industry, including Eco Flex 0040 (silicone-based), polystyrene, styrene-ethylene/butylene-styrene (SEBS), and others [81–84]. The strain tolerances of such devices have ranged from 100% to 200%, with various changes in capacitance retention. In a strained, bent, or twisted state, a decrease in the capacitance retention of the fibers is observed due to the loss of a buckled contact, reducing the available pathway for electron diffusion. Additionally, the coating of a PVA-based gel electrolyte seals the two interfaces without any issues of delamination caused by various deformations [83].

6.1.2. Coaxial CNT Layers with an Elastomer Core

Another method utilizing an elastomer core includes layering two super shearable CNT(ShCNT) sheets around a polydimethylsiloxane (PDMS) elastomer with PVA acting as the gel electrolyte and sealant to prevent a shortage, as demonstrated in Figure 14 [85]. This method resulted in a CNT supercapacitor in one fiber able to withstand 20,000 rad/m of twisting without significantly decreasing its capacitance retention. Minimal cracks and damage were observed to the CNT alignment in the film after twisting. The super shearable CNT film releases stress through the rearrangement of CNT fibrils instead of permanent deformation. Further information regarding the mechanical properties of the CNT fiber is displayed in Table 5.

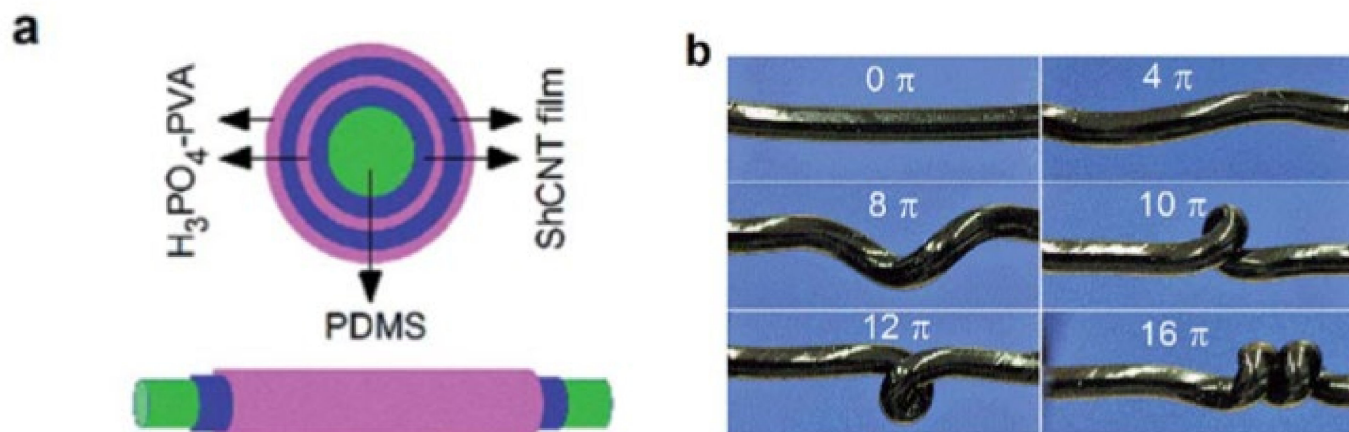


Figure 14. (a) The structure of a torsionable supercapacitor in cross-sectional and side views. (b) Digital photos showing the supercapacitor at different torsion levels. Reprinted with permission from [85].

6.1.3. Helical CNT Fibers with an Elastomer Core

An alternative method of manufacturing supercapacitors involves helically winding CNT fibers in parallel around an elastomer core. This method utilizes dry or wet spun CNT fibers, followed by doping with pseudocapacitive materials, which are then sealed with an electrolyte gel, typically a PVA solution. Symmetrical or asymmetrical fibers employing different pseudocapacitive materials are then wound helically around an elastomer core, followed by a final coat of PVA gel electrolytes to adhere to the components. The process is depicted in Figure 15 [86]. The SC in this figure is super elastic, sustaining strains as high as 850%. Varying methods produce tightly wound CNT coils with good surface contacts between the electrodes. When introduced to stress, the packing of the coils loosens, enabling movement without permanent deformation to the CNT electrodes [86–89]. The data regarding the performance of the devices under strain are summarized in Table 5.

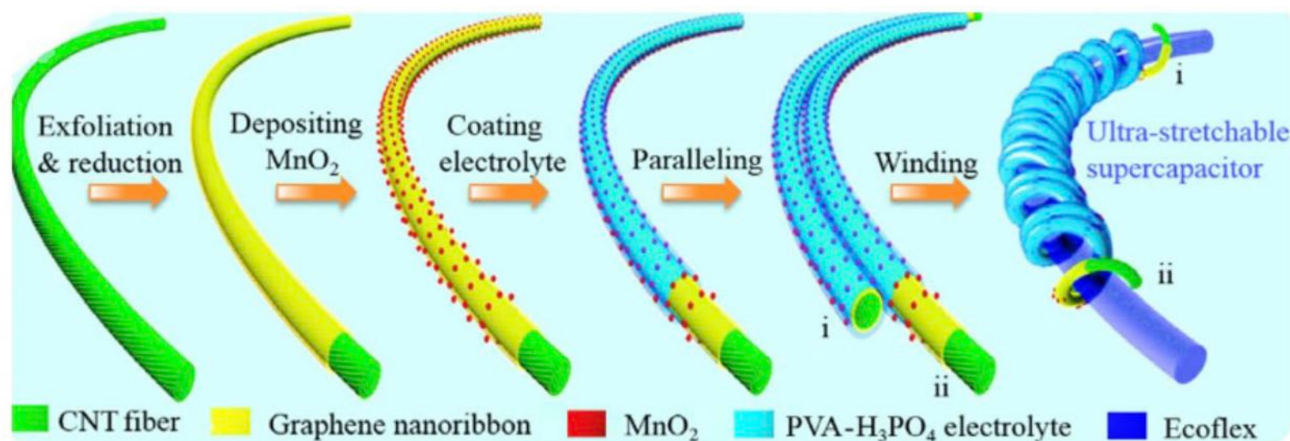


Figure 15. Schematic illustration showing the fabrication of an ultra-stretchable wire-shaped supercapacitor [86].

A modified manufacturing method for helical CNT fibers wrapped around an elastomer core was developed, demonstrating improved mechanical properties. The fibers were produced from a solution of CNTs and graphene sheets. The graphene sheet helped to create a porous structure that enhanced the ion diffusion during the electrochemical performance and contributed to its improved mechanical properties. A PVA gel electrolyte coat was applied to the individual fibers. The symmetrical electrodes were twisted together in a spring-like configuration around a temporary metal rod. The two fibers were cast in SEBS solution to provide a protective coating and to maintain a flexible spring-like design,

as depicted in Figure 16a,b. Strain rates of up to 800% without permanent deformation were demonstrated [90].

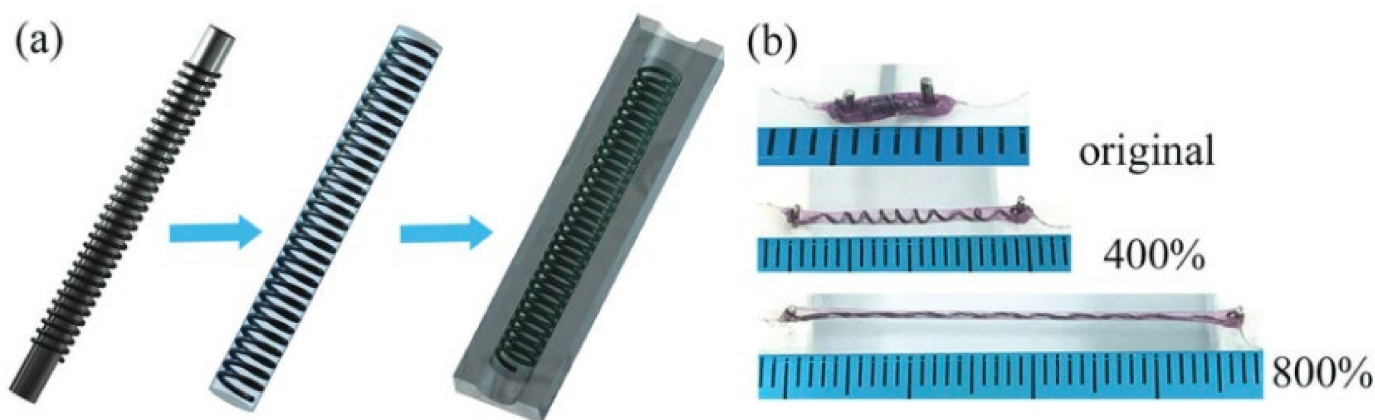


Figure 16. (a) Schematic illustration of the fabrication of an FSC in which the yarn is coiled on a rod and cast using SEBS polymer to fix the coil structure. The rod is removed, and the device is placed in a mold to cover the coil yarn with rubber. (b) Illustration of the prepared supercapacitor with different strain rates up to 800%. Reprinted with permission from [90].

6.1.4. Freestanding Helical CNT Fibers

The presence of an elastomer contributes additional weight to the CNT supercapacitors without improving the electrochemical performance. Ideally, physical configurations without elastomers are preferred but are limited due to the inherent mechanical properties of the CNT fibers. Innovative arrangements of CNT fibers have produced mechanically competitive supercapacitors [91]. Tightly coiling individual CNT fibers in a helical pattern followed by a coating of PVA allows the fibers to be elongated without damaging the connectivity. Two symmetrical CNT fibers coated with PVA can produce a freestanding helical supercapacitor (Figure 17a) with similar mechanical properties to elastomer-based supercapacitors. Figure 17b,c depict the configuration of the freestanding supercapacitor in a position of rest and elongation [92].

Two variations of the applications of this method produced CNT supercapacitors with remarkable mechanical properties. One method utilized a solution of bacteria culture (BC) cellulose structure, CNT, and poly(3,4-ethylene dioxy-thiophene) (PEDOT) to spin helically coiled fibers sealed in PVA. The PEDOT and BC support the mechanical structure while providing a highly porous surface for improved interaction with PVA [93].

The other variation utilized multiple CNT fibers spun helically, followed by a priming coat of amine groups to improve the adherence to metal–organic frameworks (MOF) grown directly on the fibers, as depicted in Figure 18. The MOF improved the mechanical integrity of the fibers while also providing a porous surface for increased diffusion of the gel electrolyte [94]. The observed mechanical properties are provided in Table 5.

6.1.5. Other Configurations

A configuration that does not fit into the general categories previously discussed is the CNT knitted coaxial supercapacitor. CNT fibers are knitted uniformly using a machine, producing a freestanding flexible structure coated in PVA. A double-walled electrode is made by sheathing one of the knitted structures inside the other to produce a single fiber for the supercapacitor (Figure 19). The drawback of such a material is the quantity of CNT fiber required to manufacture the knitted fiber. A strain of 100% was observed with minimal impact on the capacitance retention. A specific area capacitance of 511.28 mF/cm² was demonstrated [95].

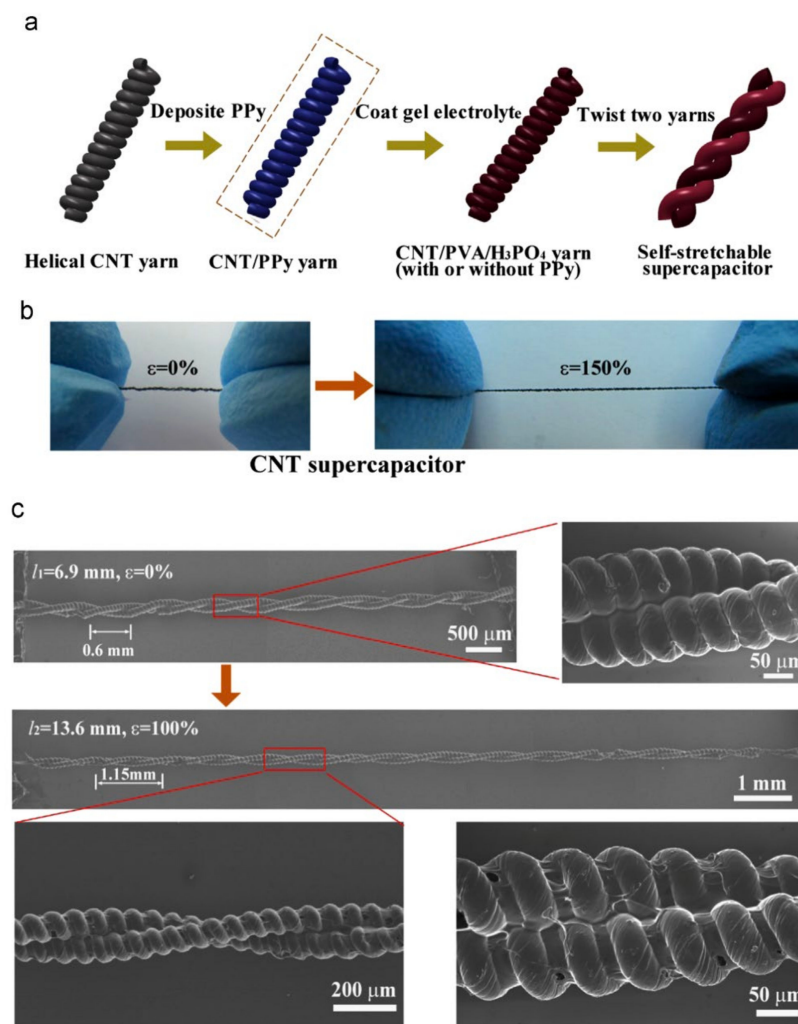


Figure 17. Fabrication of self-stretchable fiber-shaped supercapacitors. (a) Schematic of the freestanding helical CNT yarn SC fabrication process. Two of such yarns were twisted into a double-helix supercapacitor. (b) Photograph of manually stretched (1.5 times the original length) double-helix CNT yarn supercapacitor. (c) SEM images of a 6.9-mm-long supercapacitor in its original state ($l_1 = 6.9$ mm, $\epsilon = 0$) and after stretching to $l_2 = 13.6$ mm, $\epsilon = 100\%$, showing uniform deformation of helical loops and a continuous electrolyte coating on the surfaces of the yarns. Reprinted with permission from [92].



Figure 18. Schematics illustrating the synthesis process used to fabricate IRMOF3@mDWNTY (IRMOF3 = ligand-based isorecticular metal-organic framework; mDWNTY = modified double-walled nanotube yarn). Reprinted with permission from [94].

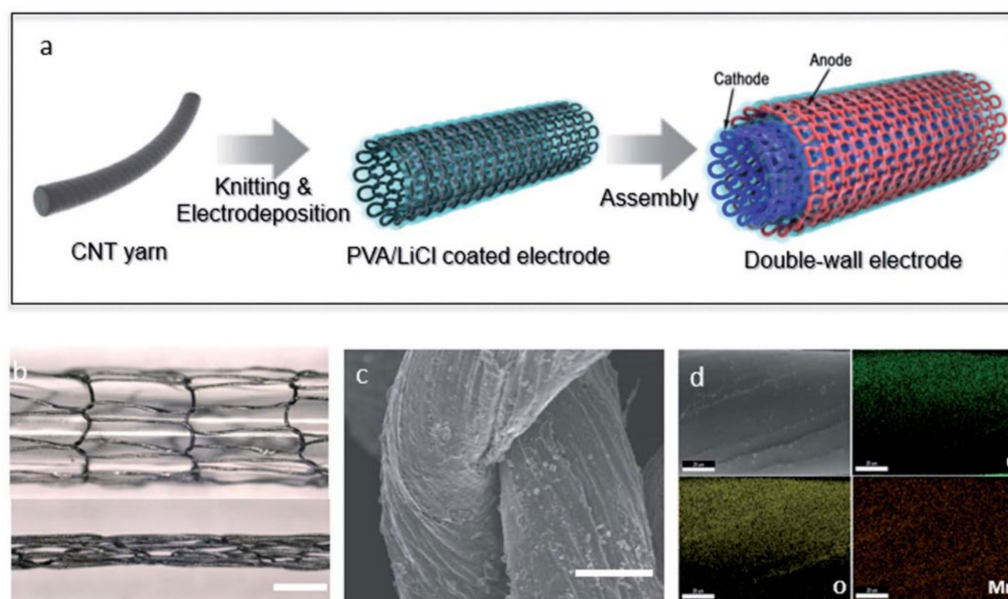


Figure 19. Schematic and images of knitted MnO_2 @CNT fiber SC. (a) Fabrication scheme of a double-walled knitted MnO_2 @CNT FSC. (b) Optical image of non-stretched ($\epsilon = 0$) and stretched ($\epsilon = 100$) knitted structures (scale bar: 1 mm). (c) SEM image of a knitted MnO_2 @CNT fiber supercapacitor (scale bar, 500 μm , and 50 μm). (d) EDX mapping images of knitted MnO_2 @CNT fiber supercapacitor (scale bar: 20 μm). Reprinted with permission from [95].

One alternative approach for a wearable supercapacitor configuration utilizes two CNT fibers arranged sinusoidally and encased in a poly(acrylamide) (PAAm) hydrogel. The latter is biocompatible, stretchable, and has excellent ionic conductivity when doped with LiCl salts. Figure 20 demonstrates the physical configuration of the CNT fibers in PAAm hydrogel [80]. This multifunctional composite can also be used as a strain sensor, as discussed in the next section.

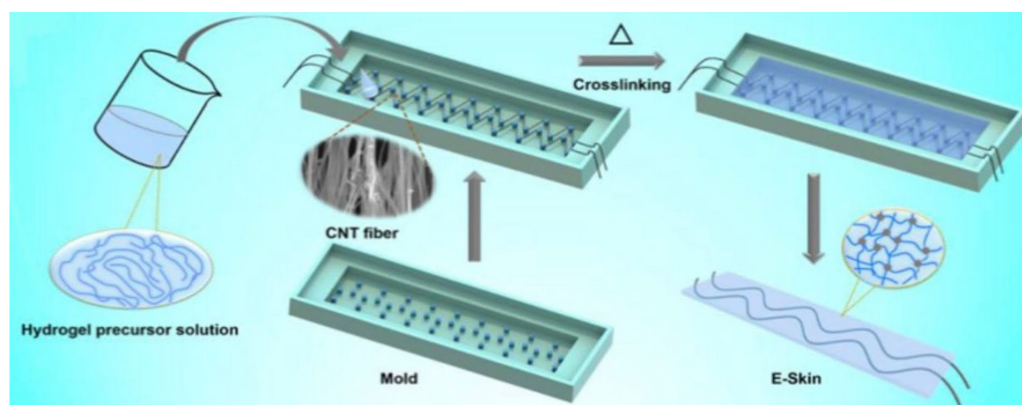


Figure 20. Schematic diagram of the CNT fiber/PAAm hydrogel (CFPH) composite preparation process. Reprinted with permission from [80].

Table 5. Summary of the stretchable supercapacitors and their characteristics, as recently reported in the literature.

Configuration	Pseudocapacitive Material/Electrolyte	Strain, Capacitance Retention	Bend, Capacitance Retention	Ultimate Strength	Capacitance	Ref
Symmetrical coiled CNT sheets, Nylon core	MnO ₂ /PVA-LiCl	150%, 88%	-	- 68 MPa	5.4 mF·cm ⁻¹ 40.9 mF·cm ⁻²	[96]
Wire-Drawn-Die-Free Standing Symmetrical Helical CNT-PPy composite fiber	PPY/PVA-H ₃ PO ₄	-	180°, 100%/100% after 1k cycles @90°	-	69 F·g ⁻¹	[91]
Free Standing Symmetrical Helical CNT yarn	PPY/PVA-H ₃ PO ₄	150%, 94%	-	-	19 F·g ⁻¹	[92]
Asymmetrical Buckled CNT sheets Eco Flex 0040 Elastomer Core	MnO ₂ /PEDOT/PVA-LiCl	200%, 97.7%	150%, 96.8%	-	2.38 mF·cm ⁻¹ 11.88 mF·cm ⁻²	[82]
Symmetrical Buckled CNT Sheets, SEBS Elastomer Core	Au and PANI/PVA-H ₃ PO ₄	400%/100% after 1k cycles	-	-	8.7 F·g ⁻¹ @1A·g ⁻¹	[81]
Asymmetrical Helical Oxidized CNT Fiber, Elastomer Core	MnO ₂ @PEDOT:PSS@OCNTF (positive) MoS ₂ @CNTF(negative) PVA-LiCl	100%, 92% after 3k cycles	-	-	278.6 mF·cm ⁻²	[87]
Symmetrical Coaxial Layered CNT Sheets, Eco flex Elastomer Core	- PVA-H ₃ PO ₄	650%, 88%	-	-	2.42–2.68 mF·cm ⁻¹	[85]
Twisted symmetrical Buckled CNT Sheets, SEBS Elastomer Core	MnO ₂ & RuO ₂ PVA-H ₃ PO ₄	200%, 100%	-	-	25.0 F·g ⁻¹	[83]
Symmetrical CNT Dipped Yarns/Ag plated Double-covered yarn polymer	(PVDF-HFP)/EMIMBF ₄	150%, 75% 5k cycles	120°, 80%, 5k cycles	46.6 MPa	4.8 F·cm ⁻³ @200 mA·cm ⁻³	[88]
Symmetrical Buckled CNT Sheets Elastomer Core	PANI PVA-H ₂ SO ₄	100%, 98%, 100 cycles	-	-	394 F·g ⁻¹	[84]
Helically Coiled CNT/Graphene Fibers, Coated in SEBS	PANI PVA-H ₃ PO ₄	800%, 99.2% 800%, 77.3%, 5k cycles	-	-	138 F·g ⁻¹	[90]
Helically Coiled Symmetrical CNT/Graphene Fibers, Eco flex Elastomer Core	MnO ₂ PVA-H ₃ PO ₄	850%, 82% after 1k cycles @ 700% strain	90°, 100%, 1k cycles	-	14.02 mF·cm ⁻²	[86]
Helically Coiled Symmetrical CNT Fibers, Spandex Elastomer Core	MnO ₂ PVA-KOH	80%, 92.1%, 500 cycles	180°, 95.3%, 500 cycles	-	685 mF·cm ⁻²	[89]
Coaxial Knitted CNT Fibers	MnO ₂ PVA-LiCl	100%, 98%, 500 cycles	160°, 100%	-	321.08 mF·cm ⁻¹ 511.28 mF·cm ⁻²	[95]
Parallel/Symmetrical Sinusoidal CNT Fibers, PAAm Hydrogel	- PAAm-LiCl	50%, 90.4%, 3k cycles	-	130 MPa	10.6 mF·cm ⁻²	[80]
Helically Coiled Symmetrical CNT Fibers, Silicone Elastomer Core	PVA-HCl	70%, 97%, 1k cycles	180°, 97%, 1k cycles	-	170 mF·cm ⁻² @100 mV·s ⁻¹	[97]
Helically Coiled Symmetrical PEDOT@BacterialCellulose (BC)/CNT Fiber	PEDOT, BC PVA-H ₃ PO ₄	1000%, 94.4%, 1k cycles	-	-	175.1 F·g ⁻¹	[93]
Helically Coiled Symmetrical CNT Fibers in Metal-Organic Framework	MOF, PVA-DMSO	-	88%, 500 cycles	492.8 MPa	225.2 F·cm ⁻³	[94]

7. Multifunctional CNT Supercapacitors

Although the review is focused on CNT fiber supercapacitors, some novel applications of these devices have also been highlighted.

7.1. Strain Sensors

One application of CNT supercapacitors lies in their tolerance to deformation, undergoing twisting and stretching while returning to an original state with negligible changes in the capacitance retention. Choi et al. manufactured an asymmetrical buckled supercapaci-

tor with a dielectric rubber core by doping both electrodes with MnO_2 , where the anode was treated with poly(3,4-ethylenedioxythipene) (PEDOT). Both electrodes were exposed to PVA-LiCl gel electrolyte around an elastomer comprised of Ecoflex 0040 [82] (Figure 21A). The supercapacitor fiber was then subjected to various twists and stretching, corresponding to a predictable change in the capacitance of the wire. The increase in capacitance was due to the decrease in fiber thickness, which increased the surface area contact between the electrodes. The device reliably displayed capacitance changes of 115.7% and 26% during elongation of 200% and twisting at 1700 rad/m, respectively (Figure 21B) [82].

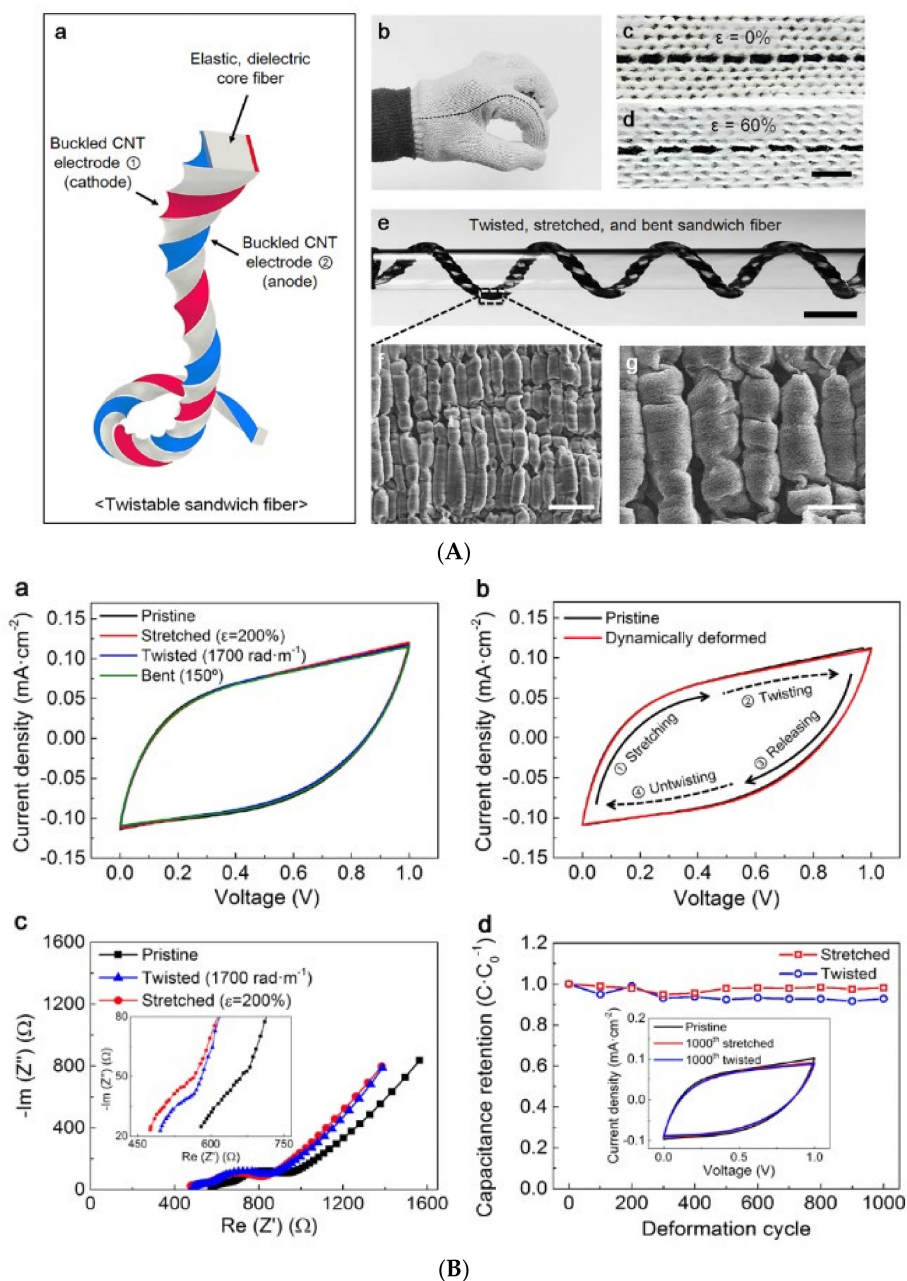


Figure 21. (A): (a) Twistable and stretchable sandwich fiber with dielectric Ecoflex 0040 rubber core and two symmetric buckled CNT electrodes. (b) Photograph of a 20 cm long sandwich fiber integrated into a glove. (c) SEM images, unstrained and (d) strained (60%) (scale bar: 8 μm); (e) photograph of the sandwich fiber wound around a 7 mm diameter glass tube (scale bar: 50 μm), with SEM images showing microscopic CNT buckles at two levels of magnification, (f) low (scale

bar: 50 μm) and (g) high (scale bar: 20 μm), which were formed during fiber relaxation from the fabrication strain. (B) Effects of severe stretching, twisting, and bending on sandwich-based fiber supercapacitors that contained MnO_2 -infiltrated buckled CNT electrodes, which were coated with 15 wt.% PVA–LiCl gel electrolytes: (a) comparison of CV curves for pristine, stretched, twisted, and bent sandwich fiber supercapacitors; (b) CV curves obtained at a scan rate of $10 \text{ mV}\cdot\text{s}^{-1}$, measured during the successive application of (i) 200% stretching, (ii) $1700 \text{ rad}\cdot\text{m}^{-1}$ twisting, (iii) release of the tensile stretching, and (iv) fiber untwisting to provide the initial state, with the CV curve before these mechanical deformations (black line) presented for comparison; (c) Nyquist curves (frequency rates range from 0.2 Hz to 100 kHz), with the inset showing the high-frequency region; (d) capacitance retention graph. The inset shows CV curves at $10 \text{ mV}\cdot\text{s}^{-1}$ measured before and after these 1000 cycles. Reprinted with permission from [82].

An alternative approach to strain sensing is to use CNT fibers as a piezoelectric harvester to generate a voltage upon the physical strain. This voltage generation is due to homochiral and heterochiral CNT fibers that twist in the opposite direction when strained. The output voltage of the fiber is dependent on the strain and was used to charge a CNT supercapacitor, showing promising potential for the application in a self-powered strain sensing device [97]. These devices are flexible and lightweight, enabling them to be incorporated into fabrics for real-time strain sensing applications.

7.2. Chromatic Supercapacitors

One novel utilization of CNT supercapacitors includes the application of fluorescent dye particles to produce electrodes that are visible in dark environments (Figure 22). Two methods of production exist, co-spinning and direct dipping. The co-spinning method involves dipping CNT sheets in a uniform aqueous solution of fluorescent dye particles before spinning the CNT fibers. The co-spinning process creates a uniform distribution of dye particles throughout the fiber. The direct dipping method includes dipping CNT fibers in a dye solution to anchor the particles to the fiber's surface. The electrochemical and mechanical properties of the dye-doped fibers are not diminished. Both methods can utilize a wide range of dye colors; however, it has been shown that the co-spinning process produces more distinguishable colors [98].

7.3. Self-Healing CNT Supercapacitors

During the wide range of motion, a break in fibers can inevitably occur in wearable electronics devices. For most of them, this can cause the failure of the entire device. Investigating the CNT supercapacitors with self-healing capabilities is a promising solution to this problem. One method of developing self-healing CNT supercapacitors involves using a self-healing polymer (SHP) fiber as a core wrapped in CNT sheets to produce a fiber electrode. The CNT/SHP fiber has self-healing properties that enable the reconnection of a broken fiber. The polymer forms hydrogen bonds between the two pieces separated via fracture sections when the two pieces are brought into contact.

Additionally, the CNTs interact via van der Waals forces. Although weak, the huge number of individual CNTs in the sections contribute to the adhesive forces. Pressing the two sections together enhances the hydrogen and van der Waals force for improved healing. In a reported study, a CNT fiber was subjected to breaking five times, displaying mechanical strength rates of 79.1% and 72.5% after the first and fifth break, respectively [99]. Two CNT self-healable polymers were twisted with PVA- H_2SO_4 as a gel electrolyte. The maximum capacitance observed with the self-healable SC was $140 \text{ F}\cdot\text{g}^{-1}$, and 92% was restored after self-healing (Figure 23A,B). The specific capacitance was assessed with and without PANI, and the SC with PANI gave a higher capacitance rate. The approach of employing self-healing polymers for the fabrication of CNT supercapacitors paves the way for improving the durability of wearable electronics.

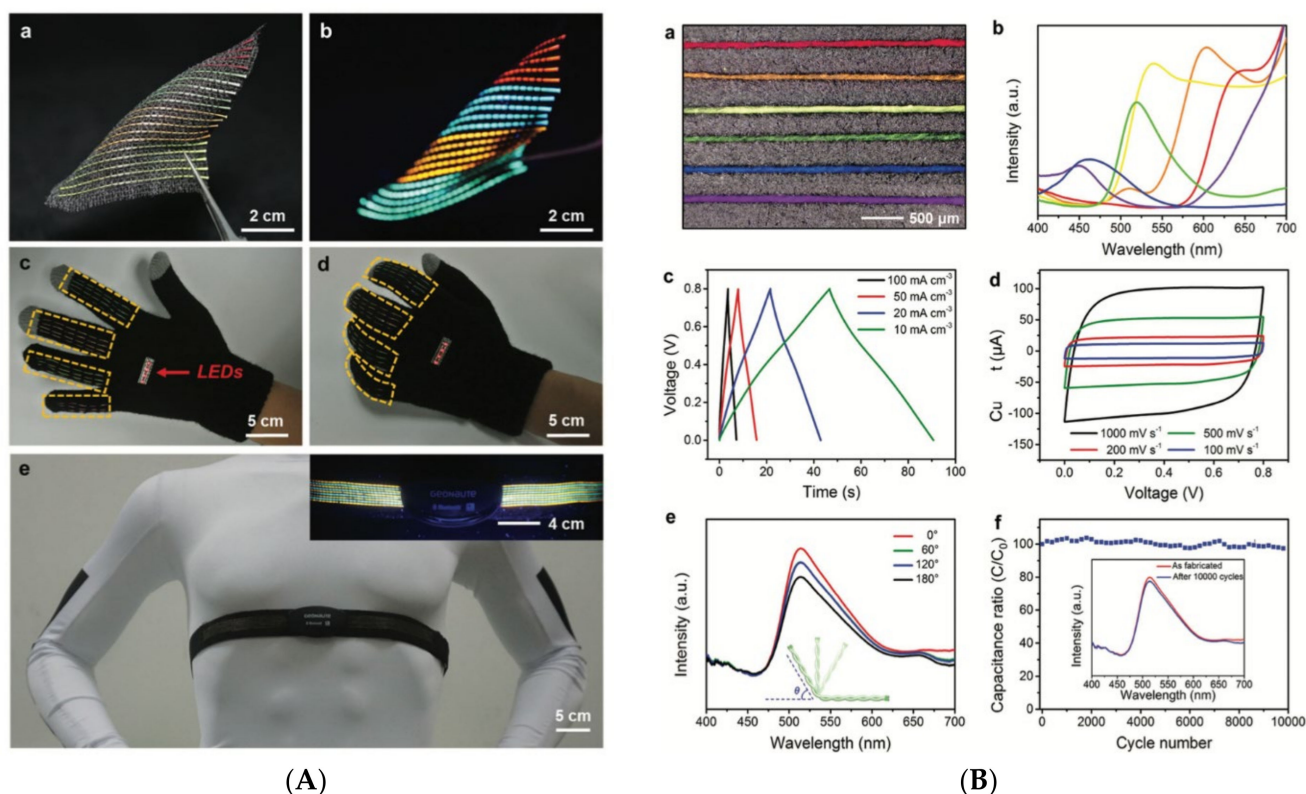


Figure 22. (A): (a,b) Photographs of twenty fluorescent supercapacitor fibers with four colors woven into a black textile under natural and ultraviolet light, respectively. (c,d) Sixteen fluorescent supercapacitor fibers are divided into four groups and woven into a glove to power four red-light-emitting diodes. (e) Eighteen fluorescent supercapacitor fibers integrated into a commercial heart rate monitoring strap to extend its running time (inset: photograph of the integrated system under ultraviolet illumination). (B): (a,b) Optical images and spectra of various colored fiber electrodes, (c) GCD curves of fluorescent fiber SC based on bare MWCNT at various current densities, (d) CV curves at different scan rates, (e) spectra of green fluorescent SCs under various bending angles, and (f) capacitance retention rates after 10k GCD cycles. (Inset: spectrum before and after 10k GCD cycles). Reproduced with permission from [98].

7.4. Shape-Retaining CNT Supercapacitors

Wearable electronics will be exposed to various strains and movements, stressing the devices. A CNT supercapacitor that relieves stress by returning to its originally intended shape is desirable to maintain the long-term health of the device. Combining a CNT supercapacitor with a shape memory polyurethane (SMP) substrate produced a device that retained its original shape, despite experiencing deformation (Figure 24A). The electrochemical performance of the shape memory polymer fiber SC (SMPFSC) is given in Figure 24B. The desired shape can be set by heating the SMP-encased CNT fiber above its transition temperature and then cooling it in the desired configuration. Various shape-retaining polymers can be used that have different transition temperatures. This process does not harm the electrochemical properties of the CNT supercapacitor. It has also been shown that the same CNT fiber can be remolded repeatedly by heating it above the transition temperature [100]. The potential for a device to be reused in various applications while also preserving the device's health is a promising application of shape retention polymers.

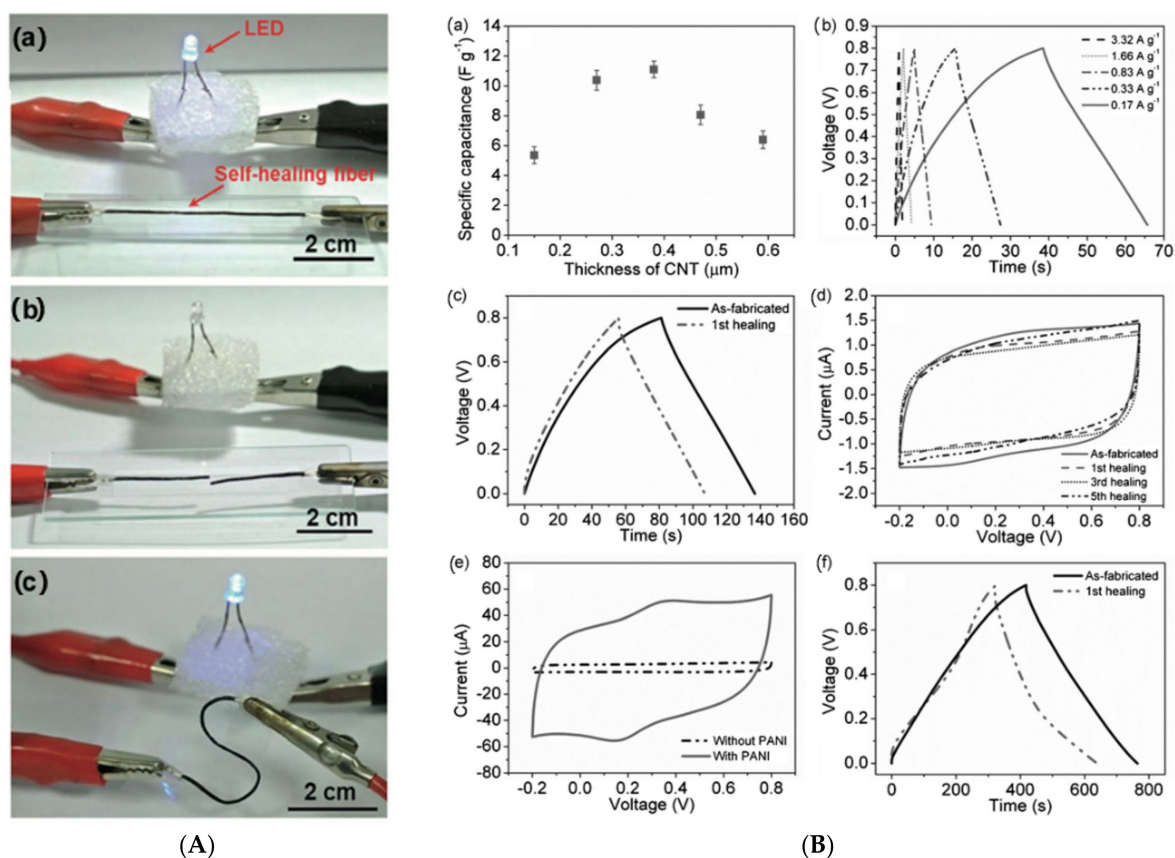


Figure 23. (A): (a–c) Photographs of a self-healing polymeric fiber (SHP) serving as a conducting wire to power a LED before breaking, after breaking, and after healing, including being bent. The voltage was set at 3.2 V. (B): (a) Dependence of the specific capacitance on the thickness of the aligned-CNT film. (b) GCD curves of a wire-shaped supercapacitor with increasing current densities at a CNT thickness of 0.38 μm . (c) GCD curves before breaking and after healing at a current density of 0.08 $A \cdot g^{-1}$. (d) CV curves at a scan rate of 50 $mV \cdot s^{-1}$ after 1, 3, and 5 healing cycles. (e) CV curves of wire-shaped supercapacitors based on aligned CNT/SHP fibers before and after incorporating PANI. (f) GCD curves for a PANI-incorporated SC before breaking and after healing at a current density of 0.17 $A \cdot g^{-1}$. Reprinted with permission from [99].

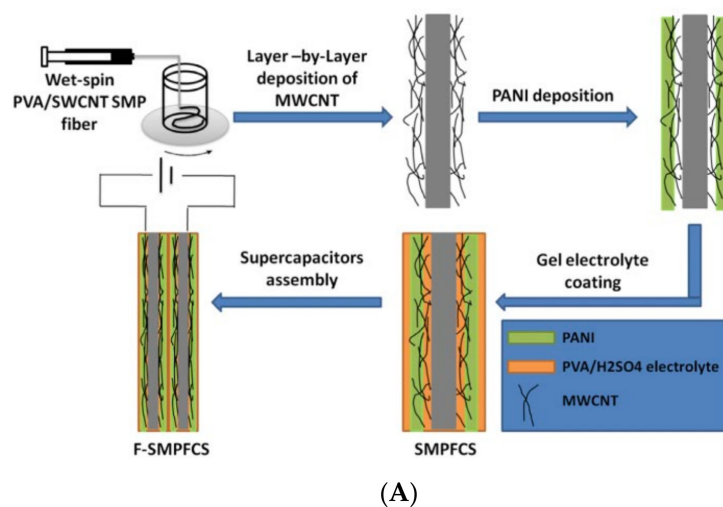


Figure 24. Cont.

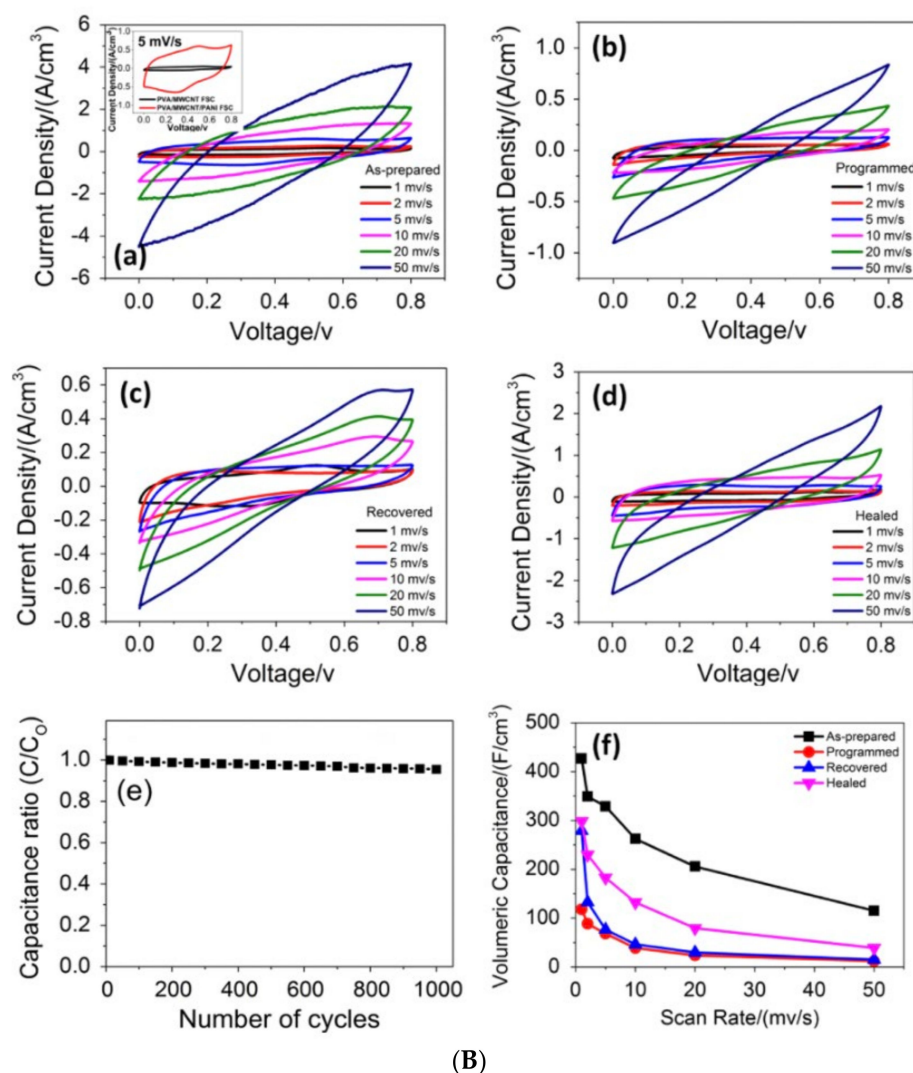


Figure 24. (A) Schematics of the fabrication process for a full shape memory polymer fiber SC (F-SMPFSC). (B) Electrochemical performance of solid-state F-SMPFSC at different shape memory cyclic stages in a two-electrode configuration. CV curves for (a) an as-prepared F-SMPFSC with the inset showing that the PANI layer can significantly increase the volumetric capacitance of SMPFCS, (b) a programmed SMPFSC with a temporary strain of 103%, (c) a recovered F-SMPFSC with a residual strain of 15%, (d) a healed F-SMPFSC obtained by immersing a recovered F-SMPFSC in a liquid $\text{H}_2\text{SO}_4/\text{PVA}$ solution for 2 h, (e) the cycle life of the F-SMPFSC (scan rate: 10 mV/s), and (f) a comparison of the volumetric capacitance rates with the scan rates at different shape memory cyclic stages. Reprinted with permission from [100].

8. Current Challenges Related to CNT-Based Fiber Supercapacitors

Despite the rapid progress, there are challenges to overcome, both in terms of the practical applications and fundamental research on wearable CNT-based and multifunctional SCs. Some of them are listed below:

- The energy densities of the CNT SCs are low compared to other energy storage devices such as microbatteries. The CNT fiber electrodes used as scaffolds and active materials, even with a high specific surface area, result in moderate energy density. This could be due to the non-accessibility of the electrolytes to the electrode. Modifying the surface area to make it electrolyte-accessible and matching the electrode's pore diameter with the electrolyte ions' size could result in higher performance. The optimization of the fiber design and configurations to ensure the complete utilization of the electrode needs to be considered;

- Most of the current wearable SC research is conducted using PVA-KOH electrolytes, as they are mechanically robust with good electrochemical stability and low costs. However, this causes the limitation of a narrow PW, resulting in a relatively low energy density. As an alternative, electrolytes with wider PWs with an organic or ionic nature can be used. Additionally, the development of new electrolytes that are safer and ionically conductive with wide PWs need to be pursued;
- Electrolytes based on sulfuric acid, phosphoric acid, and KOH are corrosive. Most research studies do not use encapsulation, making their use unsafe. Wearable SCs employing corrosive electrolytes must be encapsulated with a polymer that does not affect the device's electrochemical performance;
- The unit cost of CNT yarn is still high, which hinders the scalability and mass production of CNT-yarn-based devices. Nevertheless, inexpensive CNT fibers are expected to appear on the market in the near future;
- As wearable electronics represent a rapidly advancing field, there is a huge market for products such as smart textiles, which necessitate scalability combined with low-cost production. Moreover, the mechanical strength aspects of the CNT fibers (flexibility, stretchability, stiffness, and good endurance life after dynamic mechanical stress cycles) must match the textile standards for the satisfactory integration with the fabric via knitting, sewing, or weaving. Therefore, more collaborations between textile or garment experts and CNT fiber researchers are necessary, which will bring to life technologies that will align the CNT fibers' physical and mechanical properties with the conventional fabric materials, thereby resulting in viable wearable electronics.

9. Conclusions

The comprehensive review conducted here confirms that the CNT fibers are valuable candidates for making wearable energy storage devices. We believe that there is a huge amount of room for developing wearable CNT-based SCs and multifunctional devices. The research on using smart CNT yarns as sensors, actuators, and energy harvesters, along with integrating CNT-based SCs with advanced electronic devices, is still in its nascent stage. Breakthroughs could be accomplished in this arena via the joint efforts and insights of researchers and industrialists, supplemented by advanced materials engineering and technology developments.

Funding: This research received no external funding.

Institutional Review Board Statement: Not applicable.

Informed Consent Statement: Not applicable.

Data Availability Statement: Not applicable.

Conflicts of Interest: The authors declare no conflict of interest.

References

1. Meng, F.; Li, Q.; Zheng, L. Flexible fiber-shaped supercapacitors: Design, fabrication, and multi-functionalities. *Energy Storage Mater.* **2017**, *8*, 85–109. [[CrossRef](#)]
2. Huang, Q.; Wang, D.; Zheng, Z. Textile-Based Electrochemical Energy Storage Devices. *Adv. Energy Mater.* **2016**, *6*, 1600783. [[CrossRef](#)]
3. Chen, S.; Qiu, L.; Cheng, H.-M. Carbon-Based Fibers for Advanced Electrochemical Energy Storage Devices. *Chem. Rev.* **2020**, *120*, 2811–2878. [[CrossRef](#)] [[PubMed](#)]
4. Sun, J.; Huang, Y.; Sea, Y.N.S.; Xue, Q.; Wang, Z.; Zhu, M.; Li, H.; Tao, X.; Zhi, C.; Hu, H. Recent progress of fiber-shaped asymmetric supercapacitors. *Mater. Today Energy* **2017**, *5*, 1–14. [[CrossRef](#)]
5. Lu, Z.; Raad, R.; Safaei, F.; Xi, J.; Liu, Z.; Foroughi, J. Carbon Nanotube Based Fiber Supercapacitor as Wearable Energy Storage. *Front. Mater.* **2019**, *6*, 138. [[CrossRef](#)]
6. Conway, B.E. *Electrochemical Supercapacitors: Scientific Fundamentals and Technical Applications*; Kluwer Academic/Plenum: New York, NY, USA, 1999.
7. Senthilkumar, S.T.; Wang, Y.; Huang, H. Advances and prospects of fiber supercapacitors. *J. Mater. Chem. A* **2015**, *3*, 20863–20879. [[CrossRef](#)]

8. Xie, P.; Yuan, W.; Liu, X.; Peng, Y.; Yin, Y.; Li, Y.; Wu, Z. Advanced carbon nanomaterials for state-of-the-art flexible supercapacitors. *Energy Storage Mater.* **2020**, *36*, 56–76. [[CrossRef](#)]
9. Pan, Z.; Yang, J.; Zhang, Y.; Gao, X.; Wang, J. Quasi-solid-state fiber-shaped aqueous energy storage devices: Recent advances and prospects. *J. Mater. Chem. A* **2020**, *8*, 6406–6433. [[CrossRef](#)]
10. Cherusseri, J.; Kumar, K.S.; Choudhary, N.; Nagaiah, N.; Jung, Y.; Roy, T.; Thomas, J. Novel mesoporous electrode materials for symmetric, asymmetric and hybrid supercapacitors. *Nanotechnology* **2019**, *30*, 202001. [[CrossRef](#)] [[PubMed](#)]
11. Joseph, N.; Shafi, P.M.; Bose, A.C. Recent Advances in 2D-MoS₂ and its Composite Nanostructures for Supercapacitor Electrode Application. *Energy Fuels* **2020**, *34*, 6558–6597. [[CrossRef](#)]
12. Forouzandeh, P.; Kumaravel, V.; Pillai, S.C. Electrode Materials for Supercapacitors: A Review of Recent Advances. *Catalysts* **2020**, *10*, 969. [[CrossRef](#)]
13. Wang, J.; Li, F.; Zhu, F.; Schmidt, O.G. Recent Progress in Micro-Supercapacitor Design, Integration, and Functionalization. *Small Methods* **2018**, *3*, 1800367. [[CrossRef](#)]
14. Dong, L.; Xu, C.; Li, Y.; Huang, Z.-H.; Kang, F.; Yang, Q.-H.; Zhao, X. Flexible electrodes and supercapacitors for wearable energy storage: A review by category. *J. Mater. Chem. A* **2016**, *4*, 4659–4685. [[CrossRef](#)]
15. Yang, P.; Mai, W. Flexible solid-state electrochemical supercapacitors. *Nano Energy* **2014**, *8*, 274–290. [[CrossRef](#)]
16. Yang, Z.; Ren, J.; Zhang, Z.; Chen, X.; Guan, G.; Qiu, L.; Zhang, Y.; Peng, H. Recent Advancement of Nanostructured Carbon for Energy Applications. *Chem. Rev.* **2015**, *115*, 5159–5223. [[CrossRef](#)] [[PubMed](#)]
17. Beguin, F.; Frackowiak, E.; Gogotsi, Y. *Carbons for Electrochemical Energy Storage and Conversion Systems*; CRC Press: Boca Raton, FL, USA, 2009. [[CrossRef](#)]
18. Frackowiak, E.; Abbas, Q.; Béguin, F. Carbon/carbon supercapacitors. *J. Energy Chem.* **2013**, *22*, 226–240. [[CrossRef](#)]
19. Chen, D.; Jiang, K.; Huang, T.; Shen, G. Recent Advances in Fiber Supercapacitors: Materials, Device Configurations, and Applications. *Adv. Mater.* **2019**, *32*, e1901806. [[CrossRef](#)] [[PubMed](#)]
20. Zhang, X.; Chen, X.; Bai, T.; You, X.-Y.; Zhao, X.; Liu, X.-Y.; Ye, M.-D. Recent advances in flexible fiber-shaped supercapacitors. *Acta Phys. Sin.* **2020**, *69*, 178201. [[CrossRef](#)]
21. Jang, Y.; Kim, S.M.; Spinks, G.M.; Kim, S.J. Carbon Nanotube Yarn for Fiber-Shaped Electrical Sensors, Actuators, and Energy Storage for Smart Systems. *Adv. Mater.* **2019**, *32*, 1902670. [[CrossRef](#)] [[PubMed](#)]
22. Yao, Y.; Li, N.; Lv, T.; Chen, T. Carbon Nanotube Fibers for Wearable Devices. In *Industrial Applications of Carbon Nanotubes*; Elsevier: Amsterdam, The Netherlands, 2016; pp. 347–379. [[CrossRef](#)]
23. Wang, Y.; Song, Y.; Xia, Y. Electrochemical capacitors: Mechanism, materials, systems, characterization and applications. *Chem. Soc. Rev.* **2016**, *45*, 5925–5950. [[CrossRef](#)] [[PubMed](#)]
24. Noori, A.; El-Kady, M.F.; Rahmanifar, M.S.; Kaner, R.B.; Mousavi, M.F. Towards establishing standard performance metrics for batteries, supercapacitors and beyond. *Chem. Soc. Rev.* **2019**, *48*, 1272–1341. [[CrossRef](#)] [[PubMed](#)]
25. Kumar, Y.; Rawal, S.; Joshi, B.; Hashmi, S.A. Background, fundamental understanding and progress in electrochemical capacitors. *J. Solid State Electrochem.* **2019**, *23*, 667–692. [[CrossRef](#)]
26. Vigolo, B.; Pénicaud, A.; Coulon, C.; Sauder, C.; Pailler, R.; Journet, C.; Bernier, P.; Poulin, P. Macroscopic Fibers and Ribbons of Oriented Carbon Nanotubes. *Science* **2000**, *290*, 1331–1334. [[CrossRef](#)] [[PubMed](#)]
27. Behabtu, N.; Young, C.C.; Tsentelovich, D.E.; Kleinerman, O.; Wang, X.; Ma, A.W.K.; Bengio, E.A.; Ter Waarbeek, R.F.; De Jong, J.J.; Hoogerwerf, R.E.; et al. Strong, Light, Multifunctional Fibers of Carbon Nanotubes with Ultrahigh Conductivity. *Science* **2013**, *339*, 182–186. [[CrossRef](#)] [[PubMed](#)]
28. Bucossi, A.R.; Cress, C.D.; Schauerma, C.M.; Rossi, J.E.; Puchades, I.; Landi, B.J. Enhanced Electrical Conductivity in Extruded Single-Wall Carbon Nanotube Wires from Modified Coagulation Parameters and Mechanical Processing. *ACS Appl. Mater. Interfaces* **2015**, *7*, 27299–27305. [[CrossRef](#)] [[PubMed](#)]
29. Kou, L.; Huang, T.; Zheng, B.; Han, Y.; Zhao, X.; Gopalsamy, K.; Sun, H.; Gao, C. Coaxial wet-spun yarn supercapacitors for high-energy density and safe wearable electronics. *Nat. Commun.* **2014**, *5*, 3754. [[CrossRef](#)] [[PubMed](#)]
30. Lu, Z.; Chao, Y.; Ge, Y.; Foroughi, J.; Zhao, Y.; Wang, C.; Long, H.; Wallace, G.G. High-performance hybrid carbon nanotube fibers for wearable energy storage. *Nanoscale* **2017**, *9*, 5063–5071. [[CrossRef](#)] [[PubMed](#)]
31. Li, G.-X.; Hou, P.-X.; Luan, J.; Li, J.-C.; Li, X.; Wang, H.; Shi, C.; Liu, C.; Cheng, H.-M. A MnO₂ nanosheet/single-wall carbon nanotube hybrid fiber for wearable solid-state supercapacitors. *Carbon* **2018**, *140*, 634–643. [[CrossRef](#)]
32. Kim, J.H.; Lee, J.M.; Park, J.W.; Kim, K.J.; Kim, S.J. MnO₂/PtNP Embedded Wet-Spun Fiber Supercapacitors. *Adv. Mater. Technol.* **2018**, *3*, 1800184. [[CrossRef](#)]
33. Meng, Q.; Wang, K.; Guo, W.; Fang, J.; Wei, Z.; She, X. Thread-like Supercapacitors Based on One-Step Spun Nanocomposite Yarns. *Small* **2014**, *10*, 3187–3193. [[CrossRef](#)] [[PubMed](#)]
34. Zheng, T.; Wang, X.; Liu, Y.; Bayaniahangar, R.; Li, H.; Lu, C.; Xu, N.; Yao, Z.; Qiao, Y.; Zhang, D.; et al. Polyaniline-decorated hyaluronic acid-carbon nanotube hybrid microfiber as a flexible supercapacitor electrode material. *Carbon* **2019**, *159*, 65–73. [[CrossRef](#)]
35. Garcia-Torres, J.; Crean, C. Multilayered Flexible Fibers with High Performance for Wearable Supercapacitor Applications. *Adv. Sustain. Syst.* **2017**, *2*, 1700143. [[CrossRef](#)]
36. Koziol, K.; Vilatela, J.; Moiala, A.; Motta, M.; Cunniff, P.; Sennett, M.; Windle, A. High-Performance Carbon Nanotube Fiber. *Science* **2007**, *318*, 1892–1895. [[CrossRef](#)]

37. Li, Y.-L.; Kinloch, I.A.; Windle, A.H. Direct Spinning of Carbon Nanotube Fibers from Chemical Vapor Deposition Synthesis. *Sci. China Technol. Sci.* **2004**, *304*, 276–278. [[CrossRef](#)]
38. Shanov, V.; Cho, W.; Malik, R.; Alvarez, N.; Haase, M.; Ruff, B.; Kienzle, N.; Ochmann, T.; Mast, D.; Schulz, M. CVD growth, characterization and applications of carbon nanostructured materials. *Surf. Coat. Technol.* **2013**, *230*, 77–86. [[CrossRef](#)]
39. Cho, W.; Schulz, M.; Shanov, V. Growth and characterization of vertically aligned centimeter long CNT arrays. *Carbon* **2014**, *72*, 264–273. [[CrossRef](#)]
40. Shanov, V.N.; Schulz, M.J. Method of Growing Carbon Nanotube and Forming a Carbon Nanotube Thread Espacenet. Spinning Patent US9796121B2, 24 October 2017.
41. Alvarez, N.T.; Miller, P.; Haase, M.; Kienzle, N.; Zhang, L.; Schulz, M.J.; Shanov, V. Carbon nanotube assembly at near-industrial natural-fiber spinning rates. *Carbon* **2015**, *86*, 350–357. [[CrossRef](#)]
42. Kanakaraj, S.N.; Alvarez, N.T.; Gbordzoe, S.; Lucas, M.S.; Maruyama, B.; Noga, R.; Hsieh, Y.-Y.; Shanov, V. Improved dry spinning process at elevated temperatures for making uniform and high strength CNT fibers. *Mater. Res. Express* **2018**, *5*, 065036. [[CrossRef](#)]
43. Li, S.; Zhang, X.; Zhao, J.; Meng, F.; Xu, G.; Yong, Z.; Jia, J.; Zhang, Z.; Li, Q. Enhancement of carbon nanotube fibres using different solvents and polymers. *Compos. Sci. Technol.* **2012**, *72*, 1402–1407. [[CrossRef](#)]
44. Tran, T.; Fan, Z.; Liu, P.; Myint, S.M.; Duong, H. Super-strong and highly conductive carbon nanotube ribbons from post-treatment methods. *Carbon* **2016**, *99*, 407–415. [[CrossRef](#)]
45. Lima, M.D.; Fang, S.; Lepřo, X.; Lewis, C.; Ovalle-Robles, R.; Carretero-González, J.; Castillo-Martínez, E.; Kozlov, M.E.; Oh, J.; Rawat, N.; et al. Biscrolling Nanotube Sheets and Functional Guests into Yarns. *Science* **2011**, *331*, 51–55. [[CrossRef](#)] [[PubMed](#)]
46. Lee, J.A.; Shin, M.K.; Kim, S.H.; Cho, H.U.; Spinks, G.M.; Wallace, G.; Lima, M.D.; Lepřo, X.; Kozlov, M.E.; Baughman, R.H.; et al. Ultrafast charge and discharge biscrolled yarn supercapacitors for textiles and microdevices. *Nat. Commun.* **2013**, *4*, 1970. [[CrossRef](#)] [[PubMed](#)]
47. Queirós, G.; Rey-Raap, N.; Pereira, C.; Pereira, M.F.R. CNT-based Materials as Electrodes for Flexible Supercapacitors. *U. Porto J. Eng.* **2021**, *7*, 151–162. [[CrossRef](#)]
48. Beidaghi, M.; Gogotsi, Y. Capacitive energy storage in micro-scale devices: Recent advances in design and fabrication of micro-supercapacitors. *Energy Environ. Sci.* **2014**, *7*, 867–884. [[CrossRef](#)]
49. Su, F.; Miao, M. Flexible, high performance Two-Ply Yarn Supercapacitors based on irradiated Carbon Nanotube Yarn and PEDOT/PSS. *Electrochim. Acta* **2014**, *127*, 433–438. [[CrossRef](#)]
50. Adusei, P.K.; Gbordzoe, S.; Kanakaraj, S.N.; Hsieh, Y.-Y.; Alvarez, N.T.; Fang, Y.; Johnson, K.; McConnell, C.; Shanov, V. Fabrication and study of supercapacitor electrodes based on oxygen plasma functionalized carbon nanotube fibers. *J. Energy Chem.* **2019**, *40*, 120–131. [[CrossRef](#)]
51. Liang, Y.; Luo, X.; Weng, W.; Hu, Z.; Zhang, Y.; Xu, W.; Bi, Z.; Zhu, M. Activated Carbon Nanotube Fiber Fabric as a High-Performance Flexible Electrode for Solid-State Supercapacitors. *ACS Appl. Mater. Interfaces* **2021**, *13*, 28433–28441. [[CrossRef](#)]
52. Kim, J.H.; Choi, C.; Lee, J.M.; De Andrade, M.J.; Baughman, R.H.; Kim, S.J. Ag/MnO₂ Composite Sheath-Core Structured Yarn Supercapacitors. *Sci. Rep.* **2018**, *8*, 1–8. [[CrossRef](#)]
53. Zhou, Q.; Tang, G.; Chen, X.; Su, F. Flexible Supercapacitors Based on CNT/MnO₂-BP Composite Yarn Synthesized by In Situ Reduction. *J. Electrochem. Soc.* **2021**, *168*, 080524. [[CrossRef](#)]
54. Zhou, Q.; Chen, X.; Su, F.; Lyu, X.; Miao, M. Sandwich-Structured Transition Metal Oxide/Graphene/Carbon Nanotube Composite Yarn Electrodes for Flexible Two-Ply Yarn Supercapacitors. *Ind. Eng. Chem. Res.* **2020**, *59*, 5752–5759. [[CrossRef](#)]
55. Le, T.S.; Truong, T.K.; Huynh, V.N.; Bae, J.; Suh, D. Synergetic design of enlarged surface area and pseudo-capacitance for fiber-shaped supercapacitor yarn. *Nano Energy* **2019**, *67*, 104198. [[CrossRef](#)]
56. Jian, X.; Li, H.; Li, H.; Li, Y.; Shang, Y. Flexible and freestanding MoS₂/rGO/CNT hybrid fibers for high-capacity all-solid supercapacitors. *Carbon* **2020**, *172*, 132–137. [[CrossRef](#)]
57. Shi, P.; Li, L.; Hua, L.; Qian, Q.; Wang, P.; Zhou, J.; Sun, G.; Huang, W. Design of Amorphous Manganese Oxide@Multiwalled Carbon Nanotube Fiber for Robust Solid-State Supercapacitor. *ACS Nano* **2016**, *11*, 444–452. [[CrossRef](#)] [[PubMed](#)]
58. He, Y.; Chen, W.; Gao, C.; Zhou, J.; Li, X.; Xie, E. An overview of carbon materials for flexible electrochemical capacitors. *Nanoscale* **2013**, *5*, 8799–8820. [[CrossRef](#)]
59. Wang, Q.; Wu, Y.; Li, T.; Zhang, D.; Miao, M.; Zhang, A. High performance two-ply carbon nanocomposite yarn supercapacitors enhanced with a platinum filament and in situ polymerized polyaniline nanowires. *J. Mater. Chem. A* **2016**, *4*, 3828–3834. [[CrossRef](#)]
60. Wu, Y.; Wang, Q.; Li, T.; Zhang, D.; Miao, M. Fiber-shaped Supercapacitor and Electrocatalyst Containing of Multiple Carbon Nanotube Yarns and One Platinum Wire. *Electrochim. Acta* **2017**, *245*, 69–78. [[CrossRef](#)]
61. Wang, Q.; Zhang, D.; Wu, Y.; Li, T.; Zhang, A.; Miao, M. Fabrication of Supercapacitors from NiCo₂O₄Nanowire/Carbon-Nanotube Yarn for Ultraviolet Photodetectors and Portable Electronics. *Energy Technol.* **2017**, *5*, 1449–1456. [[CrossRef](#)]
62. Sun, J.; Man, P.; Zhang, Q.; He, B.; Zhou, Z.; Li, C.; Wang, X.; Guo, J.; Zhao, J.; Xie, L.; et al. Hierarchically-structured Co₃O₄ nanowire arrays grown on carbon nanotube fibers as novel cathodes for high-performance wearable fiber-shaped asymmetric supercapacitors. *Appl. Surf. Sci.* **2018**, *447*, 795–801. [[CrossRef](#)]
63. He, H.; Yang, X.; Wang, L.; Zhang, X.; Li, X.; Lü, W. Enhanced Energy Density of Coaxial Fiber Asymmetric Supercapacitor Based on MoS₂@Fe₂O₃/Carbon Nanotube Paper and Ni(OH)₂@NiCo₂O₄/Carbon Nanotube Fiber Electrodes. *Chem.—A Eur. J.* **2020**, *26*, 17212–17221. [[CrossRef](#)]

64. Zhang, Q.; Xu, W.; Sun, J.; Pan, Z.; Zhao, J.; Wang, X.; Zhang, J.; Man, P.; Guo, J.; Zhou, Z.; et al. Constructing Ultrahigh-Capacity Zinc–Nickel–Cobalt Oxide@Ni(OH)₂ Core–Shell Nanowire Arrays for High-Performance Coaxial Fiber-Shaped Asymmetric Supercapacitors. *Nano Lett.* **2017**, *17*, 7552–7560. [[CrossRef](#)]
65. Sun, J.; Zhang, Q.; Wang, X.; Zhao, J.; Guo, J.; Zhou, Z.; Zhang, J.; Man, P.; Sun, J.; Li, Q.; et al. Constructing hierarchical dandelion-like molybdenum–nickel–cobalt ternary oxide nanowire arrays on carbon nanotube fiber for high-performance wearable fiber-shaped asymmetric supercapacitors. *J. Mater. Chem. A* **2017**, *5*, 21153–21160. [[CrossRef](#)]
66. Huang, G.; Zhang, Y.; Wang, L.; Sheng, P.; Peng, H. Fiber-based MnO₂/carbon nanotube/polyimide asymmetric supercapacitor. *Carbon* **2017**, *125*, 595–604. [[CrossRef](#)]
67. Zong, Q.; Zhang, Q.; Mei, X.; Li, Q.; Zhou, Z.; Li, D.; Chen, M.; Shi, F.; Sun, J.; Yao, Y.; et al. Facile Synthesis of Na-Doped MnO₂ Nanosheets on Carbon Nanotube Fibers for Ultrahigh-Energy-Density All-Solid-State Wearable Asymmetric Supercapacitors. *ACS Appl. Mater. Interfaces* **2018**, *10*, 37233–37241. [[CrossRef](#)]
68. Liu, J.-H.; Xu, X.-Y.; Yu, J.; Hong, J.-L.; Liu, C.; Ouyang, X.; Lei, S.; Meng, X.; Tang, J.-N.; Chen, D.-Z. Facile construction of 3D porous carbon nanotubes/polypyrrole and reduced graphene oxide on carbon nanotube fiber for high-performance asymmetric supercapacitors. *Electrochim. Acta* **2019**, *314*, 9–19. [[CrossRef](#)]
69. Kim, J.; Yu, H.; Jung, J.Y.; Kim, M.J.; Jeon, D.; Jeong, H.S.; Kim, N.D. 3D Architecturing Strategy on the Utmost Carbon Nanotube Fiber for Ultra-High Performance Fiber-Shaped Supercapacitor. *Adv. Funct. Mater.* **2022**, *32*, 2113057. [[CrossRef](#)]
70. Adusei, P.K.; Johnson, K.; Kanakaraj, S.N.; Zhang, G.; Fang, Y.; Hsieh, Y.-Y.; Khosravifar, M.; Gbordzoe, S.; Nichols, M.; Shanov, V. Asymmetric Fiber Supercapacitors Based on a FeC₂O₄/FeOOH-CNT Hybrid Material. *C* **2021**, *7*, 62. [[CrossRef](#)]
71. Mirabedini, A.; Lu, Z.; Mostafavian, S.; Foroughi, J. Triaxial Carbon Nanotube/Conducting Polymer Wet-Spun Fibers Supercapacitors for Wearable Electronics. *Nanomaterials* **2020**, *11*, 3. [[CrossRef](#)] [[PubMed](#)]
72. Liu, N.; Pan, Z.; Ding, X.; Yang, J.; Xu, G.; Li, L.; Wang, Q.; Liu, M.; Zhang, Y. In-situ growth of vertically aligned nickel cobalt sulfide nanowires on carbon nanotube fibers for high capacitance all-solid-state asymmetric fiber-supercapacitors. *J. Energy Chem.* **2019**, *41*, 209–215. [[CrossRef](#)]
73. Xu, T.; Yang, D.; Liu, Y.; Zhang, S.; Zhang, M.; Zhao, T.; Li, X.; Yu, Z.-Z. Hierarchical Transition Metal Oxide Arrays Grown on Graphene-Based Fibers with Enhanced Interface by Thin Layer of Carbon toward Solid-State Asymmetric Supercapacitors. *ChemElectroChem* **2020**, *7*, 1860–1868. [[CrossRef](#)]
74. Kanakaraj, S.N.; Hsieh, Y.-Y.; Adusei, P.K.; Homan, B.; Fang, Y.; Zhang, G.; Mishra, S.; Gbordzoe, S.; Shanov, V. Nitrogen-doped CNT on CNT hybrid fiber as a current collector for high-performance Li-ion capacitors. *Carbon* **2019**, *149*, 407–418. [[CrossRef](#)]
75. Liang, X.; Wang, Q.; Ma, Y.; Zhang, D. A high performance asymmetric supercapacitor based on in situ prepared CuCo₂O₄ nanowires and PPY nanoparticles on a two-ply carbon nanotube yarn. *Dalton Trans.* **2018**, *47*, 17146–17152. [[CrossRef](#)] [[PubMed](#)]
76. Man, P.; Zhang, Q.; Sun, J.; Guo, J.; Wang, X.; Zhou, Z.; He, B.; Li, Q.; Xie, L.; Zhao, J.; et al. Hierarchically structured VO₂@PPy core-shell nanowire arrays grown on carbon nanotube fibers as advanced cathodes for high-performance wearable asymmetric supercapacitors. *Carbon* **2018**, *139*, 21–28. [[CrossRef](#)]
77. Guo, J.; Zhang, Q.; Sun, J.; Li, C.; Zhao, J.; Zhou, Z.; He, B.; Wang, X.; Man, P.; Li, Q.; et al. Direct growth of vanadium nitride nanosheets on carbon nanotube fibers as novel negative electrodes for high-energy-density wearable fiber-shaped asymmetric supercapacitors. *J. Power Sources* **2018**, *382*, 122–127. [[CrossRef](#)]
78. Li, T.; Wu, Y.; Wang, Q.; Zhang, D.; Zhang, A.; Miao, M. TiO₂ crystalline structure and electrochemical performance in two-ply yarn CNT/TiO₂ asymmetric supercapacitors. *J. Mater. Sci.* **2017**, *52*, 7733–7743. [[CrossRef](#)]
79. Xu, Y.; Yan, Y.; Lu, W.; Yarlagadda, S.; Xu, G. High-Performance Flexible Asymmetric Fiber-Shaped Supercapacitor Based on CF/PPy and CNT/MnO₂ Composite Electrodes. *ACS Appl. Energy Mater.* **2021**, *4*, 10639–10645. [[CrossRef](#)]
80. Yi, F.-L.; Meng, F.-C.; Li, Y.-Q.; Huang, P.; Hu, N.; Liao, K.; Fu, S.-Y. Highly stretchable CNT Fiber/PAAm hydrogel composite simultaneously serving as strain sensor and supercapacitor. *Compos. Part B Eng.* **2020**, *198*, 108246. [[CrossRef](#)]
81. Zhu, W.; Zhang, Y.; Zhou, X.; Xu, J.; Liu, Z.; Yuan, N.; Ding, J. Miniaturized Stretchable and High-Rate Linear Supercapacitors. *Nanoscale Res. Lett.* **2017**, *12*, 448. [[CrossRef](#)] [[PubMed](#)]
82. Choi, C.; Lee, J.M.; Kim, S.H.; Kim, S.J.; Di, J.; Baughman, R.H. Twistable and Stretchable Sandwich Structured Fiber for Wearable Sensors and Supercapacitors. *Nano Lett.* **2016**, *16*, 7677–7684. [[CrossRef](#)] [[PubMed](#)]
83. Lee, D.W.; Lee, J.H.; Min, N.K.; Jin, J.-H. Buckling Structured Stretchable Pseudocapacitor Yarn. *Sci. Rep.* **2017**, *7*, 12005. [[CrossRef](#)] [[PubMed](#)]
84. Ren, D.; Dong, L.; Wang, J.; Ma, X.; Xu, C.; Kang, F. Facile Preparation of High-Performance Stretchable Fiber-Like Electrodes and Supercapacitors. *ChemistrySelect* **2018**, *3*, 4179–4184. [[CrossRef](#)]
85. Meng, F.; Zheng, L.; Luo, S.; Li, D.; Wang, G.; Jin, H.; Li, Q.; Zhang, Y.; Liao, K.; Cantwell, W.J. A highly torsionable fiber-shaped supercapacitor. *J. Mater. Chem. A* **2017**, *5*, 4397–4403. [[CrossRef](#)]
86. Wang, H.; Wang, C.; Jian, M.; Wang, Q.; Xia, K.; Yin, Z.; Zhang, M.; Liang, X.; Zhang, Y. Superelastic wire-shaped supercapacitor sustaining 850% tensile strain based on carbon nanotube@graphene fiber. *Nano Res.* **2017**, *11*, 2347–2356. [[CrossRef](#)]
87. Zhang, Q.; Sun, J.; Pan, Z.; Zhang, J.; Zhao, J.; Wang, X.; Zhang, C.; Yao, Y.; Lu, W.; Li, Q.; et al. Stretchable fiber-shaped asymmetric supercapacitors with ultrahigh energy density. *Nano Energy* **2017**, *39*, 219–228. [[CrossRef](#)]
88. Shi, M.; Yang, C.; Song, X.; Liu, J.; Zhao, L.; Zhang, P.; Gao, L. Stretchable wire-shaped supercapacitors with high energy density for size-adjustable wearable electronics. *Chem. Eng. J.* **2017**, *322*, 538–545. [[CrossRef](#)]

89. Zheng, X.; Zhou, X.; Xu, J.; Zou, L.; Nie, W.; Hu, X.; Dai, S.; Qiu, Y.; Yuan, N. Highly stretchable CNT/MnO₂ nanosheets fiber supercapacitors with high energy density. *J. Mater. Sci.* **2020**, *55*, 8251–8263. [[CrossRef](#)]
90. Lu, Z.; Foroughi, J.; Wang, C.; Long, H.; Wallace, G.G. Superelastic Hybrid CNT/Graphene Fibers for Wearable Energy Storage. *Adv. Energy Mater.* **2017**, *8*, 1702047. [[CrossRef](#)]
91. Guo, F.M.; Xu, R.Q.; Cui, X.; Zhang, L.; Wang, K.L.; Yao, Y.W.; Wei, J.Q. High performance of stretchable carbon nanotube–polypyrrole fiber supercapacitors under dynamic deformation and temperature variation. *J. Mater. Chem. A* **2016**, *4*, 9311–9318. [[CrossRef](#)]
92. Shang, Y.; Wang, C.; He, X.; Li, J.; Peng, Q.; Shi, E.; Wang, R.; Du, S.; Cao, A.; Li, Y. Self-stretchable, helical carbon nanotube yarn supercapacitors with stable performance under extreme deformation conditions. *Nano Energy* **2015**, *12*, 401–409. [[CrossRef](#)]
93. Liang, Q.; Wan, J.; Ji, P.; Zhang, D.; Sheng, N.; Chen, S.; Wang, H. Continuous and integrated PEDOT@Bacterial cellulose/CNT hybrid helical fiber with “reinforced cement-sand” structure for self-stretchable solid supercapacitor. *Chem. Eng. J.* **2021**, *427*, 131904. [[CrossRef](#)]
94. Na, Y.W.; Cheon, J.Y.; Kim, J.H.; Jung, Y.; Lee, K.; Park, J.S.; Park, J.Y.; Song, K.S.; Lee, S.B.; Kim, T.; et al. All-in-one flexible supercapacitor with ultrastable performance under extreme load. *Sci. Adv.* **2022**, *8*, eabl8631. [[CrossRef](#)] [[PubMed](#)]
95. Park, T.; Jang, Y.; Park, J.W.; Kim, H.; Kim, S.J. Quasi-solid-state highly stretchable circular knitted MnO₂@CNT supercapacitor. *RSC Adv.* **2020**, *10*, 14007–14012. [[CrossRef](#)]
96. Choi, C.; Kim, S.H.; Sim, H.J.; Lee, J.A.; Choi, A.Y.; Kim, Y.T.; Lepro, X.; Spinks, G.M.; Baughman, R.H.; Kim, S.J. Stretchable, Weavable Coiled Carbon Nanotube/MnO₂/Polymer Fiber Solid-State Supercapacitors. *Sci. Rep.* **2015**, *5*, 9387. [[CrossRef](#)] [[PubMed](#)]
97. Mun, T.J.; Kim, S.H.; Park, J.W.; Moon, J.H.; Jang, Y.; Huynh, C.; Baughman, R.H.; Kim, S.J. Wearable Energy Generating and Storing Textile Based on Carbon Nanotube Yarns. *Adv. Funct. Mater.* **2020**, *30*, 2000411. [[CrossRef](#)]
98. Liao, M.; Sun, H.; Zhang, J.; Wu, J.; Xie, S.; Fu, X.; Sun, X.; Wang, B.; Peng, H. Multicolor, Fluorescent Supercapacitor Fiber. *Small* **2017**, *14*, e1702052. [[CrossRef](#)] [[PubMed](#)]
99. Sun, H.; You, X.; Jiang, Y.; Guan, G.; Fang, X.; Deng, J.; Chen, P.; Luo, Y.; Peng, H. Self-Healable Electrically Conducting Wires for Wearable Microelectronics. *Angew. Chem. Int. Ed.* **2014**, *53*, 9526–9531. [[CrossRef](#)] [[PubMed](#)]
100. Zhong, J.; Meng, J.; Yang, Z.; Poulin, P.; Koratkar, N. Shape memory fiber supercapacitors. *Nano Energy* **2015**, *17*, 330–338. [[CrossRef](#)]